



# WPI

## **Investigating Fetch-Limited Wave Growth in the Coastal Alaskan Arctic**

A Major Qualifying Project

Submitted to the Faculty of

WORCESTER POLYTECHNIC INSTITUTE

in partial fulfillment of the requirements for the

Degree of Bachelor of Science in Physics

By

Michelle Sangillo

April 25, 2024

Submitted to:

Professor Nancy Burnham

Worcester Polytechnic Institute

Doctor Maddie Smith

Woods Hole Oceanographic Institution

*This report represents the work of one or more WPI undergraduate students submitted to the faculty as evidence of completion of a degree requirement. WPI routinely publishes these reports on the web without editorial or peer review.*

# Abstract

Climate change is affecting sea ice extent and thickness in the Arctic, which disproportionately affects coastal Alaskan communities. Thus, understanding relationships between the atmosphere, ice, and ocean in coastal regions is necessary. The effect of spatial variation of fetches on the development of waves in the coastal Arctic was investigated using wave observations from three seafloor moorings, ERA5 atmospheric reanalysis, and NASA Worldview satellite imagery. The results indicate fetch-limited wave growth between mooring locations. Waves are more developed with distance from shore, and correspond to longer fetch lengths, especially for onshore winds. Overall, this indicates that fetch size limits wave growth and drives variability among coastal Arctic locations.

# Acknowledgements

I would like to thank Dr. Nancy Burnham for her continuous support, guidance, and curiosity throughout this project, as well as Dr. Maddie Smith for her invaluable expertise and support. Additionally, thank you to Dr. Jim Thomson and Dr. Maddie Smith (supported by NSF OPP-2214651) for early access to the mooring data used here. I would also like to thank the Woods Hole Oceanographic Institution for the many generous opportunities that they have offered to me, including my WHOI Summer Student Fellowship (SSF), which laid the foundation for this research, under NSF REU OCE-2150401 and my SSF Travel Award to the Ocean Sciences Meeting 2024 in New Orleans, Louisiana. I thank the WPI Physics Department for supporting my travel as well. And thank you to the crew of the R/V Tioga for showing me the ropes of mooring deployment.

## Table of Contents

Abstract .....	i
Acknowledgements .....	ii
1. Introduction .....	1
2. Literature Review .....	4
2.1. Waves .....	4
2.1.1. Wave terminology .....	6
2.1.2. Wind-driven wave growth .....	7
2.1.3. Duration and fetch-limited waves .....	9
2.2. Sea ice .....	10
2.2.1. Growth and breakup cycle .....	12
2.3. Wave-ice interactions .....	16
2.3.1. Wave growth in sea ice .....	16
2.3.2. Wave attenuation by sea ice .....	18
2.3.3. Waves in landfast sea ice zones .....	19
3. Methodology .....	20
3.1. Datasets .....	20
3.1.1. Moorings in the Arctic .....	20
3.1.2. Atmospheric reanalysis .....	23
3.1.3. Satellite imagery .....	23
3.2. Derived parameters .....	24
3.2.1. Empirical fetch calculations .....	24
3.2.2. Wave age calculations .....	25
3.3. Data analysis .....	25
4. Results .....	27
4.1. Summary of observed wave and atmospheric conditions .....	27
4.2. Fetch .....	29
4.2.1. Fetch-limited growth from the coast .....	29
4.3. Wave age .....	31
4.3.1. Onshore and offshore winds .....	32
4.3.2. Comparing locations .....	35
5. Conclusions and future work .....	37

5.1. Future work.....	37
6. References.....	39

# 1. Introduction

Climate change is harming our Earth, especially in the polar regions. In the Arctic, the coverage, thickness, and compactness of sea ice is decreasing (Squire, 2007, 2020). In 2023, the Arctic ice cap reached the 6<sup>th</sup> lowest measured minimum sea ice extent since 1979 at 4.23 million square kilometers (Meier, 2023). Sea ice is crucial for regulating heat and ocean circulation (*Why Sea Ice Matters*, n.d.), as the bright white of ice and snow reflects sunlight back into space. With less sea ice, more heat is being absorbed by Earth, increasing the temperature and reducing ice extent, creating a vicious cycle (US EPA, 2016).

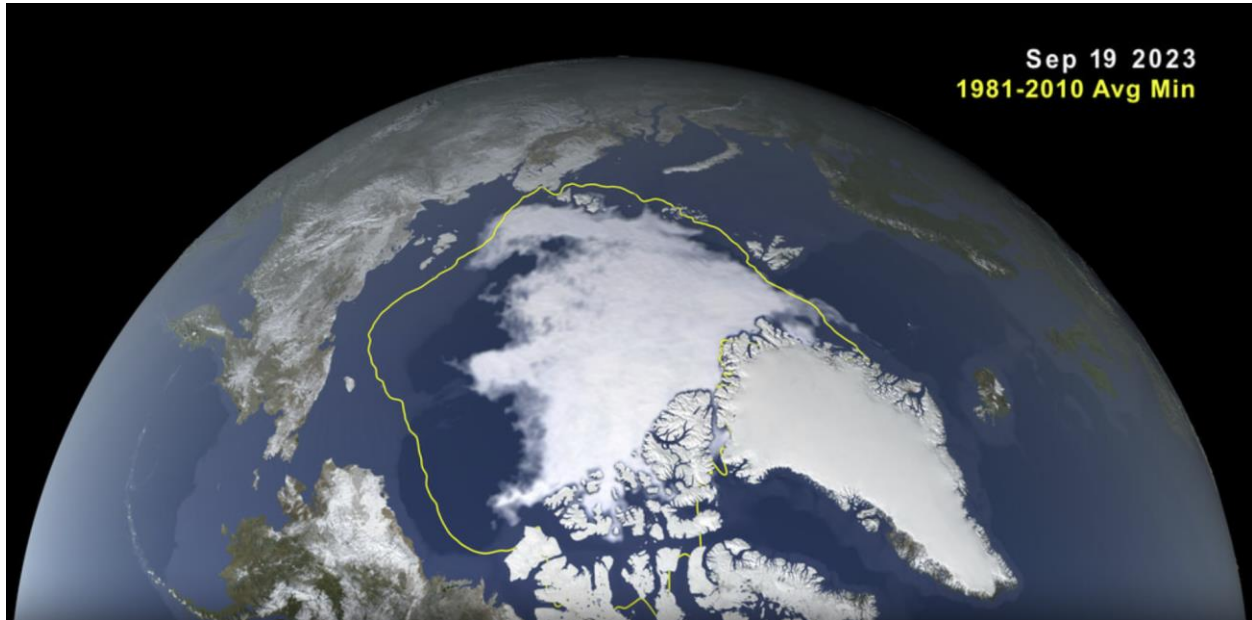


*Figure 1. Arctic sea ice follows an annual cycle of freeze-up and melt. The Arctic ice cap melts to its “minimum” every summer before increasing with the onset of colder weather. In 2023, the ice cap likely reached its minimum on Sept. 19<sup>th</sup>, pictured here. The yellow boundary marks the minimum extent averaged from 1981 to 2010 (10 yrs) (Meier, 2023).*

The Arctic is warming at two to three times the rate of the rest of the world (*Why Sea Ice Matters*, n.d.). With global warming, there is a documented global uptrend of winds and wave amplitudes, which is most severe at high latitudes, like the Arctic (Squire, 2020). Destructive storms with high amplitude waves are becoming more common which are able to penetrate further into sea ice, affecting the way sea ice forms and breaks up (Squire, 2007, 2020). This destructive power weakens the sea ice and is beginning to change the distribution of floe sizes. As floes are typically smaller, the summer sea ice in the Arctic is evolving to be less compact and becoming more similar to that in the Southern Ocean around Antarctica (Squire, 2020). Ice fields are more open with less compact ice, which create larger open water distances over which waves can grow, feeding into a cycle of growing wave heights (Squire, 2020).

There are two main categories of sea ice in the Arctic: drifting pack ice, which covers most of the basin, and landfast sea ice, which is thick sea ice attached to coastlines. As part of the effect

of global warming, landfast sea ice extent and duration are decreasing (Mahoney, 2018). This disproportionately affects coastal Arctic communities that rely on the ice in their daily lives. Landfast sea ice is the most accessible form of sea ice and the most encountered by people (Mahoney, 2018). Coastal communities on the Arctic North Slope travel across landfast sea ice to fish at the seaward edge and hunt mammals and birds for sustenance (Figure 2a & b). The oil and gas industry also travel across the ice on ice roads to access nearshore production and exploration facilities (Figure 2c) (Mahoney, 2018).



*Figure 2. Landfast sea ice is used by many people for sustenance and travel. (a) Whaling crews make camp on the landfast sea ice (Brewster, n.d.). (b) Hunters use the ice edge to hunt and fish (Brewster, n.d.). (c) Local communities use the landfast sea ice to travel on ice roads (on right of image) and the oil and gas industry travel across the ice for access to nearshore production and exploration facilities (Mahoney, 2018). Image courtesy of Jim Thomson.*

With the Arctic gaining more global attention, as a result of climate change (Squire, 2020), support for more air-sea-ice interactions research in the Arctic is growing. Ocean physics research helps to fill this need by studying the physical processes and conditions in the ocean. Using a variety of tools, including data science, climate models, and satellite and sub-orbital data ocean physicists study ocean and climate dynamics, sea level rise, the hydrological cycle, and ocean interactions (*Ocean Physics at NASA - NASA Science*, n.d.). Since Earth's oceans absorb, store, and transport large quantities of heat, water, moisture, and carbon dioxide, they shape Earth's climate and weather (*Ocean Physics at NASA - NASA Science*, n.d.). Air-sea interactions and waves are important components of the global role of oceans. One method to investigate

these two components is the use of seafloor moorings, which are anchors that hold instruments at a certain location. Moorings provide the wave observations for this research. Figure 3 pictures the author helping to deploy a similar mooring to those used here aboard the R/V Tioga, a Woods Hole Oceanographic Institution coastal-class research vessel.



*Figure 3. The author (right) participating in the deployment of seafloor moorings, similar to the ones used in this analysis, off the coast of Martha’s Vineyard, MA in Nov., 2023, aboard the R/V Tioga, Woods Hole Oceanographic Institution’s small, fast coastal research vessel (“R/V Tioga - Woods Hole Oceanographic Institution,” n.d.). Image courtesy of Maddie Smith.*

This report explores how spatial variation of fetches affects the development of waves in the coastal Arctic. First, a review of literature provides background information on waves, the niche environment of the Arctic, and how they interact. The methodology follows, including descriptions of the three datasets used. Then the results of the analysis are discussed. Lastly, the report closes with conclusions and a discussion of avenues for future work.

## 2. Literature Review

This chapter provides a detailed examination of waves and sea ice in the Arctic. The review is divided into three sections focusing on both waves and sea ice individually and closing with how they interact with one another in the Arctic. Ocean waves are characterized, and their growth described temporally and spatially. This is followed by the characterization of sea ice, with a focus on landfast sea ice, which leads into the sea ice's growth and breakup cycle in the Arctic. Finally, wave-ice interactions are discussed including wave growth and attenuation in sea ice, ending with a description of the knowledge gap.

### 2.1. Waves

Waves, ranging from tiny wavelets to tidal waves, form on all bodies of water. There are three main mechanisms that form waves. Gravitational attraction of the moon and the sun, the first mechanism, results in waves with the longest periods of 12 and 24 hours that manifest as tides (*New to Waves?*, n.d.). Waves with periods of one minute to three hours tend to be caused by natural phenomenon such as storms, earthquakes, volcanic eruptions, and landslides (NOAA, 2023). The third mechanism is wind (NOAA, 2023). Wind-driven waves tend to have periods ranging from one second to 30 seconds, encompassing a significant portion of wave energy as demonstrated in Figure 4. Wind-driven wave growth is described in Section 2.1.2. Waves are also categorized by their restoring forces (Figure 4). These are the forces that work to restore the surface to its calm equilibrium condition after it has been disturbed. Gravity acts as the restoring force for the low frequency waves (Webb, 2023). Thus, they are designated gravity waves, not to be confused with gravitational waves in astrophysics. Capillary waves are high frequency waves, where surface tension is the restoring force (Webb, 2023). Ultra gravity waves fall in between gravity and capillary waves and are restored by a combination of gravity and surface tension (Webb, 2023). Most wind waves are gravity waves.

Waves move through the water, transmitting energy rather than mass. The water moves up, down, and side to side, but it does not travel with the waves (NOAA, 2023). Instead, orbital velocities form beneath the wave as it propagates, attenuating with depth. Figure 5 demonstrates the orbital shapes in deep waters where the bottom does not interfere. In shallower depths where the orbital velocities do not have the distance to fully attenuate, the orbital velocities become more elliptical with the vertical minor axis decreasing with depth, until the motion is all back and forth at the bottom (*New to Waves?*, n.d.).

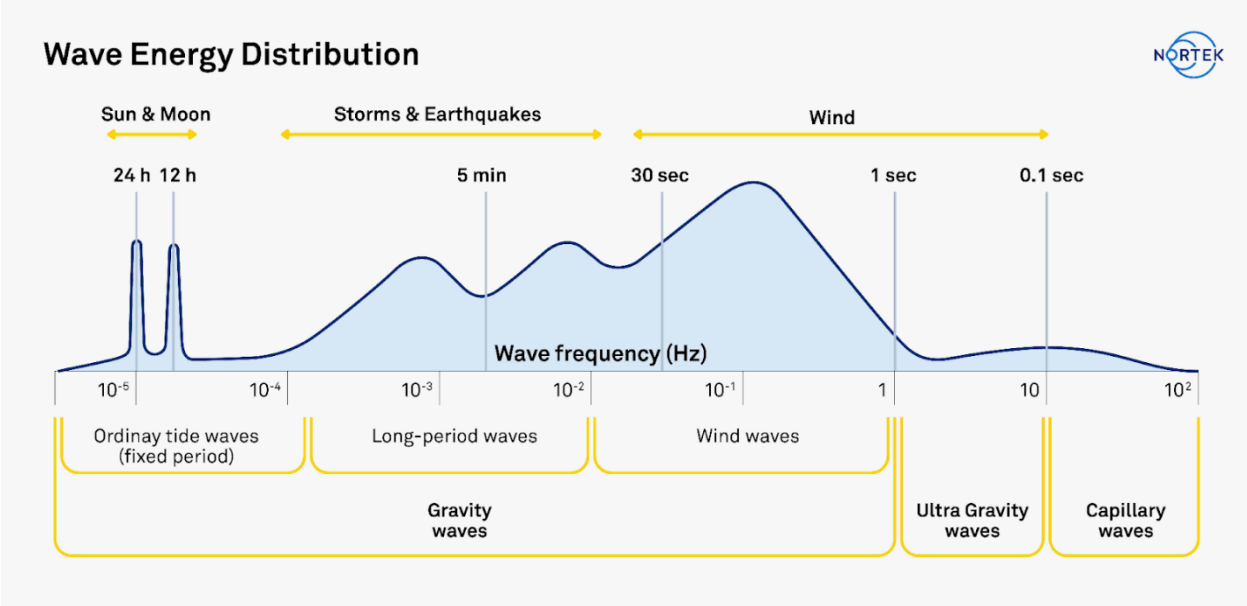


Figure 4. A distribution of relative energy (blue shaded area) based on the wave frequency, displaying wave types, generating forces, and frequencies, in Hz, or periods. Period is the inverse of frequency,  $T = 1/f$  (New to Waves?, n.d.).

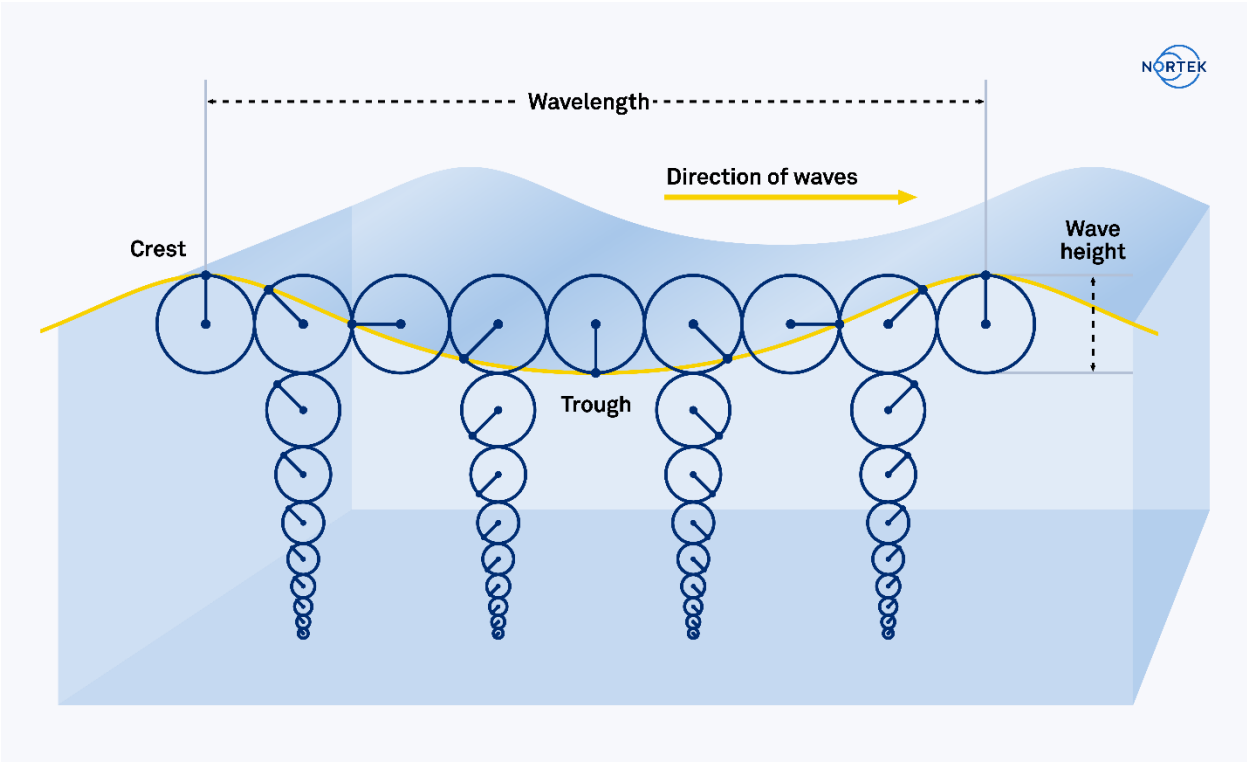


Figure 5. As waves propagate in deep water, wave orbits form beneath the wave as demonstrated. The orbital velocities attenuate with depth (New to Waves?, n.d.).

### 2.1.1. Wave terminology

Gravity waves are typically characterized by bulk parameters that describe the energy and scales of waves. The conventional physics terms for waves still apply with the addition of specific terminology to characterize the more chaotic nature of the ocean's surface. Basic wave components include the still water level, which is the surface level with no waves present. The *amplitude* of the wave is half of the *wave height*, which is the difference between the *crest* or highest point of the wave, and the *trough* or lowest point of the wave. *Wavelength* is the distance between two identical points on successive waves. The ratio of wave height to wavelength, called *wave steepness*, determines if the wave will break. If the wave steepness exceeds 1/7, the wave is too steep and will break. Wave motion is described by its *period* which is the time taken for two successive crests to pass a given point, *frequency* which is the inverse of the period and expresses the number of waves passing a point in an amount of time, often a second, and *celerity* which describes how fast the wave is traveling as the product of wavelength and frequency. *Phase* is also useful in comparing waves as it specifies the location of a point within a wave cycle and determines how they will interfere (Webb, 2023).

Since the ocean surface is covered in many wind waves with different frequencies, directions, phases, and amplitudes, ranging from a centimeter scale for ripples to a meter scale for larger swells, bulk parameters help to characterize the ocean surface. *Wave energy spectra* show the distribution of the wave spectral density [ $\text{m}^2/\text{Hz}$ ], often referred to as wave energy, with frequency [Hz]. Since the energy of the waves at a specific frequency is proportional to the square of the amplitude of the waves at that frequency, the spectrum of the energy distributed with frequency of a train of waves is directly related to the distribution of wave amplitudes with frequency (Raichlen, 2013). Figure 6 demonstrates the shape of two wave spectra, one at a time with off-ice winds and the other with on-ice winds. The energy of both peaks around 0.105 Hz and 0.110 Hz (Smith & Thomson, 2016a). The corresponding periods of 9.52 s and 9.09 s are called the *peak wave periods*, as they are associated with the most energetic waves in the wave spectrum (National Weather Service, 2018).

*Significant wave heights* refer to the wave heights of the larger, more significant waves. The term was originally coined to refer to the mean height of the highest third of the waves because visual estimates of wave heights' done by investigators at the Scripps Institute correlated well with this average (Raichlen, 2013). Since then, significant wave height is often defined as four times the standard deviation of the surface elevation (Squire, 2020). These bulk parameters along with the conventional physical terminology help describe the complex ocean surface.

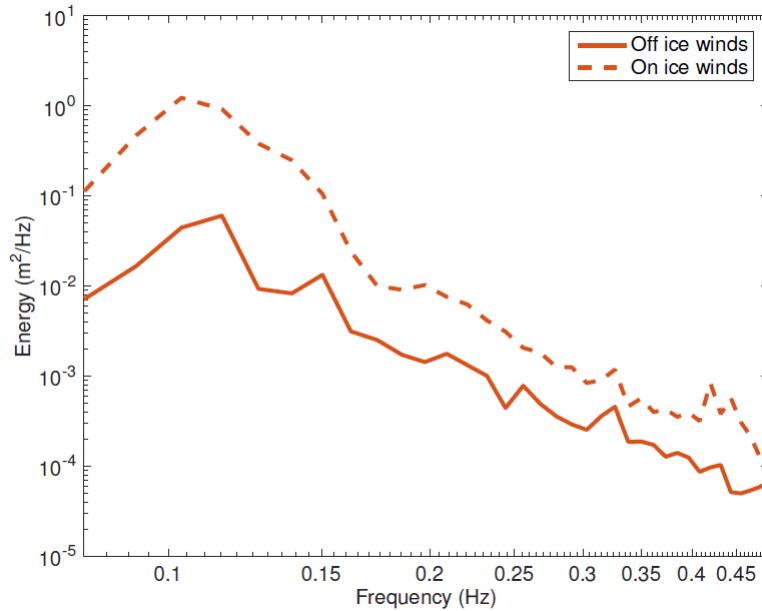


Figure 6. Two wave spectra at different times to show the general shape of the energy distribution of waves with frequency (Smith & Thomson, 2016a).

### 2.1.2. Wind-driven wave growth

Wind is the main mechanism that forms ocean surface gravity waves. Fundamentally, airflow over the ocean surface transfers energy to the ocean surface as waves. There are a few theories for how this occurs at different stages of the growth process.

In the earliest stage of wave growth, where ripples begin to form on a quiescent surface, Phillips theory dominates. Phillips theory, after Owen Phillips, says that eddies, a turbulent component in wind, have associated pressure disturbances that do work on the water surface (Figure 7a). This generates wavelets, which can grow to waves once resonance occurs when the wavelets and pressure perturbations travel at a certain speed. This reliance on resonance between surface waves and pressure fluctuations in wind predicts that wave amplitudes grow linearly and weakly in time (Pizzo et al., 2021). Once the amplitudes of the wavelets grow to a few millimeters, other mechanisms take over. In reality, the Phillips mechanism rarely acts on the surface, since the ocean surface is seldom quiescent.

For short waves, a realistic estimate of wave growth was obtained by Stephen Belcher and Julian Hunt after building on the geometric phenomenon of sheltering, proposed by Sir Harold Jeffreys (Pizzo et al., 2021). Sheltering is the deflection of air flow over water by surface geometry. It is caused by the pressure difference between the windward (upstream) and leeward (downstream) sides of a wave. When the oscillatory wind pressure and slope of the water wave are phase-shifted with respect to each other, work is done on the wave causing it to grow. In Jeffreys original theory, there is an unconstrained scaling parameter called the sheltering coefficient. However, Jeffreys theory does not account for the sheltering coefficient's dependence on the

specific geometry, which was experimentally shown to be crucial (Pizzo et al., 2021). Based solely on the leeward side's airflow deformation, Belcher and Hunt (1993) used turbulence theory to quantify how pressure differences caused by sheltering is affected by turbulent eddies (Figure 7Figure 7b) (Pizzo et al., 2021).

For larger and longer waves, Miles' mechanism takes over. Miles' mechanism, from John Miles, uses shear-flow instability with a mean wind profile so that shear flow instability occurs at a critical height, where the wind speed matches the phase speed of the growing wave. A coupling occurs between the surface wave and its induced perturbation at the critical height, which produces waves from energy and momentum removed from the wind (Figure 7c). The curvature of the wind profile at the critical heights determines the rate of growth of the wave. Miles' mechanism dominates for larger and longer waves, however, it ignores turbulence and its effects, the effect of viscosity, and interactions of waves with short and long wavelengths (Pizzo et al., 2021).

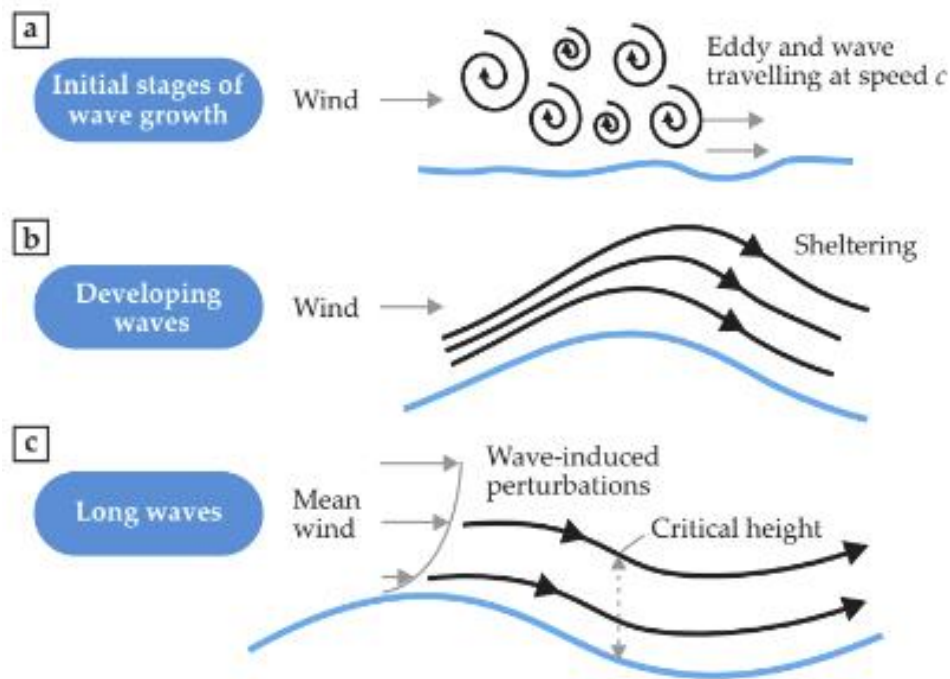


Figure 7. The mechanisms of wind-driven wave generation and growth. In the initial stages of growth, (a) turbulent eddies in the air disturb the calm ocean surface, creating ripples with wavelengths of centimeters according to Phillips theory. (b) The wavelengths of the ripples grow to the meter-scale and sheltering takes effect, caused by the pressure difference between the windward and leeward sides of the wave. (c) Once the waves are sufficiently long, the shear of the wind resonates with the wave at the critical height, transferring energy to it and causing the wave to grow (Pizzo et al., 2021).

These theoretical mechanisms, along with numerical, laboratory, and field advances, contribute to the understanding of wind-driven wave generation. However, realistic field conditions are more complex than these theories suggest, and wave-growth mechanisms are an active area of research, relying greatly on numerical models and simulations (Pizzo et al., 2021).

### 2.1.3. Duration and fetch-limited waves

Even though the theories presented in Section 2.1.2 do not capture the complexity of realistic field conditions, an empirical model of locally generated wind-driven waves is often used with realistic results. Generally, waves are generated by work the wind does on the ocean surface. Thus, through conservation of momentum and energy and the constructive nature of waves, wave growth is limited by either the time that the wind has been blowing, known as the duration, or the distance of open water over which the wind has been blowing, known as the fetch (Figure 8) (Smith & Thomson, 2016a).

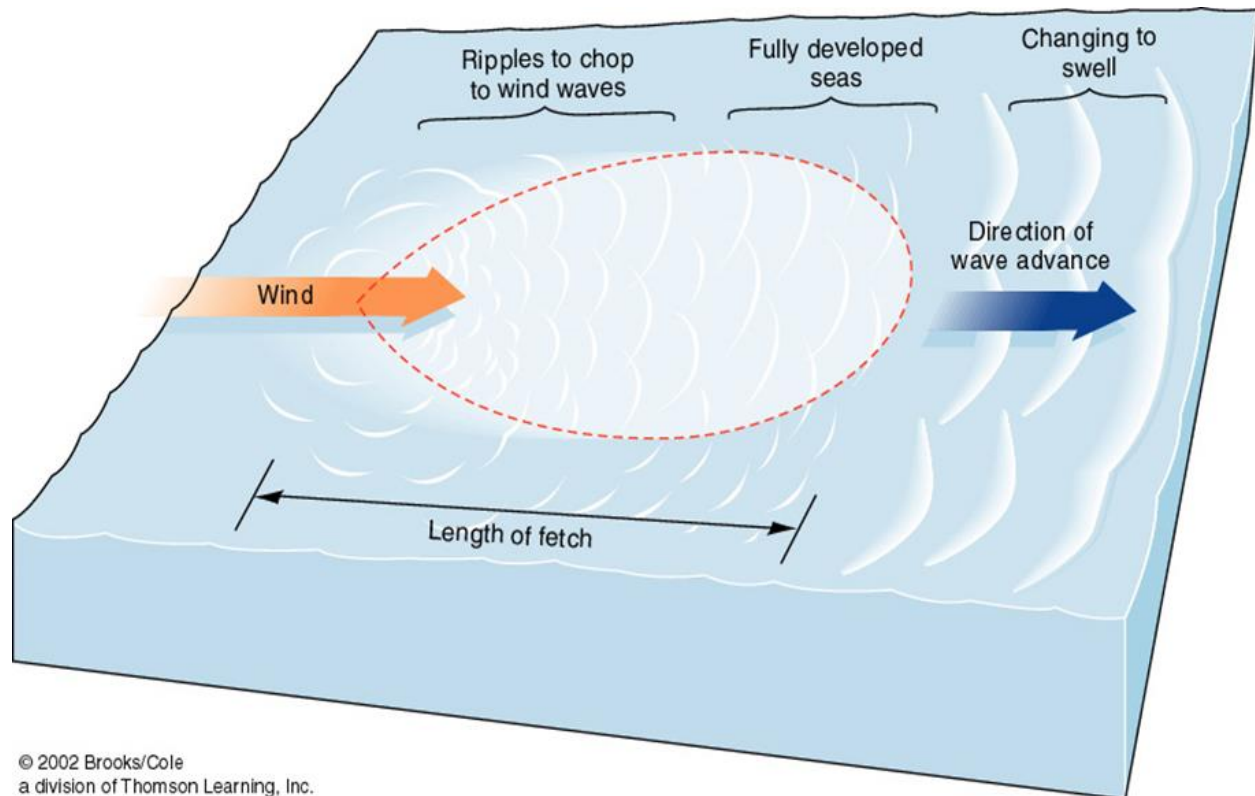


Figure 8. Diagram of the development of wind waves over a fetch, showing how shorter fetches can limited wave growth (The Geophile Pages, n.d.).

Harald Sverdrup and Walter Munk used this and simple scaling arguments to estimate wave heights based on the intensity, duration, and fetch over which the wind blew, in order to predict the heights of storm waves that crashed onto beaches near Normandy, France during D-Day (Pizzo et al., 2021). They categorized waves into two growth types, duration-limited waves and fetch-limited waves (Young, 1999). While in situ, natural wind is rarely uniform and steady as idealized here, the equations are often in agreement with observations (Thomson & Rogers, 2014; Young, 1999). These relationships are still used conceptually to understand wave evolution processes and are implicitly used by global wave models (M. Smith, personal communication, December 20, 2023). They utilize four nondimensional variables of energy, frequency, fetch, and duration:

$$\varepsilon = \frac{g^2 H_s^2}{16U^4} \quad \text{- nondimensional energy,} \quad 2.1$$

$$v = \frac{U f_e}{g} \quad \text{- nondimensional frequency,} \quad 2.2$$

$$\chi = \frac{gx}{U^2} \quad \text{- nondimensional fetch, \&} \quad 2.3$$

$$\varsigma = \frac{gt}{U} \quad \text{- nondimensional duration,} \quad 2.4$$

where  $g$  is acceleration due to gravity,  $H_s$  is significant wave height,  $U$  is wind speed,  $f_e$  is energy-weighted average frequency,  $x$  is dimensional open water distance, and  $t$  is wind duration (Young, 1999). According to empirical studies in a wide range of conditions, nondimensional energy scales well with nondimensional distance. Thus, when the nondimensional fetch is plotted against the nondimensional energy and fit with

$$\varepsilon = A\chi^a, \quad 2.5$$

$A$  falls in the  $1.6 \times 10^{-7}$  to  $1.3 \times 10^{-6}$  range and  $a$  in the 0.75 to 1.00 range (Smith & Thomson, 2016a). Although idealized, these relations are conceptually critical and often agree with observations.

## 2.2. Sea ice

Ice is a complex material that protects Earth and its inhabitants, globally and locally. It serves as a crucial part of Earth's cooling system. The wide expanses of ice and snow in the Arctic and Antarctic reflect sunlight that would otherwise warm the Earth (US EPA, 2016). Sea ice can also protect coastlines and local communities against the harsh and energetic ocean. There are two main types of ice, sea ice and freshwater ice. Within these categories there are many types of ice, each with their own important characteristics. Here, sea ice is the focus.

The Arctic is full of dynamic ice floes and ringed by stationary ice. Ice floes, not to be confused with icebergs, which are large masses of freshwater sourced ice broken from glaciers or ice shelves that float out to sea, come in many different sizes and their movement is controlled by the wind, waves, and currents. Often the floes will group together into drifting pack ice. Larger floes generally form in the center, decreasing in size towards the edges of the pack where the destructive power of the waves is stronger. Pack ice interacts with itself as well as the stationary ice attached to the land (Mahoney, 2018).

There are two principal ways sea ice attaches to land. The first is landlocked ice that forms in lagoons, fjords, channels, and enclosed waters (Figure 9). There are no dynamic forces in these locations, so the ice remains undeformed and level (Mahoney, 2018). The second is landfast sea ice.



*Figure 9. Flaw leads, or areas of open water between landfast sea ice and pack ice, can help distinguish the dynamic and stationary ice from one another (Mahoney, 2018).*

Landfast sea ice forms along open coasts wherever sea ice occurs and holds fast to the shoreline. On the seaward edge, the landfast sea ice is exposed to the ocean. Depending on the conditions, a stretch of open water can develop between the seaward edge and pack ice, called a flaw lead. If the pack ice is right at the seaward edge, the pack ice interacts with landfast sea ice, and the dynamic forces cause the ice to converge and pile up into pressure ridges above and below the landfast sea ice (Figure 9). In some cases, deep ridges cause the sea ice to fasten to the sea floor (Mahoney, 2018).

Forming most often on the coasts of Russia and in the Canadian Arctic Archipelago (Figure 10), landfast sea ice in the Arctic makes up approximately 12% of Northern Hemisphere's total wintertime sea ice coverage by typically extending an average annual maximum of 1.8 million km<sup>2</sup> (Mahoney, 2018). The local extent depends on the bathymetry, or water depth, and keel depth, or lowest point beneath the water, with seaward edges often found in 15-30 m of water in the Arctic (Mahoney, 2018).

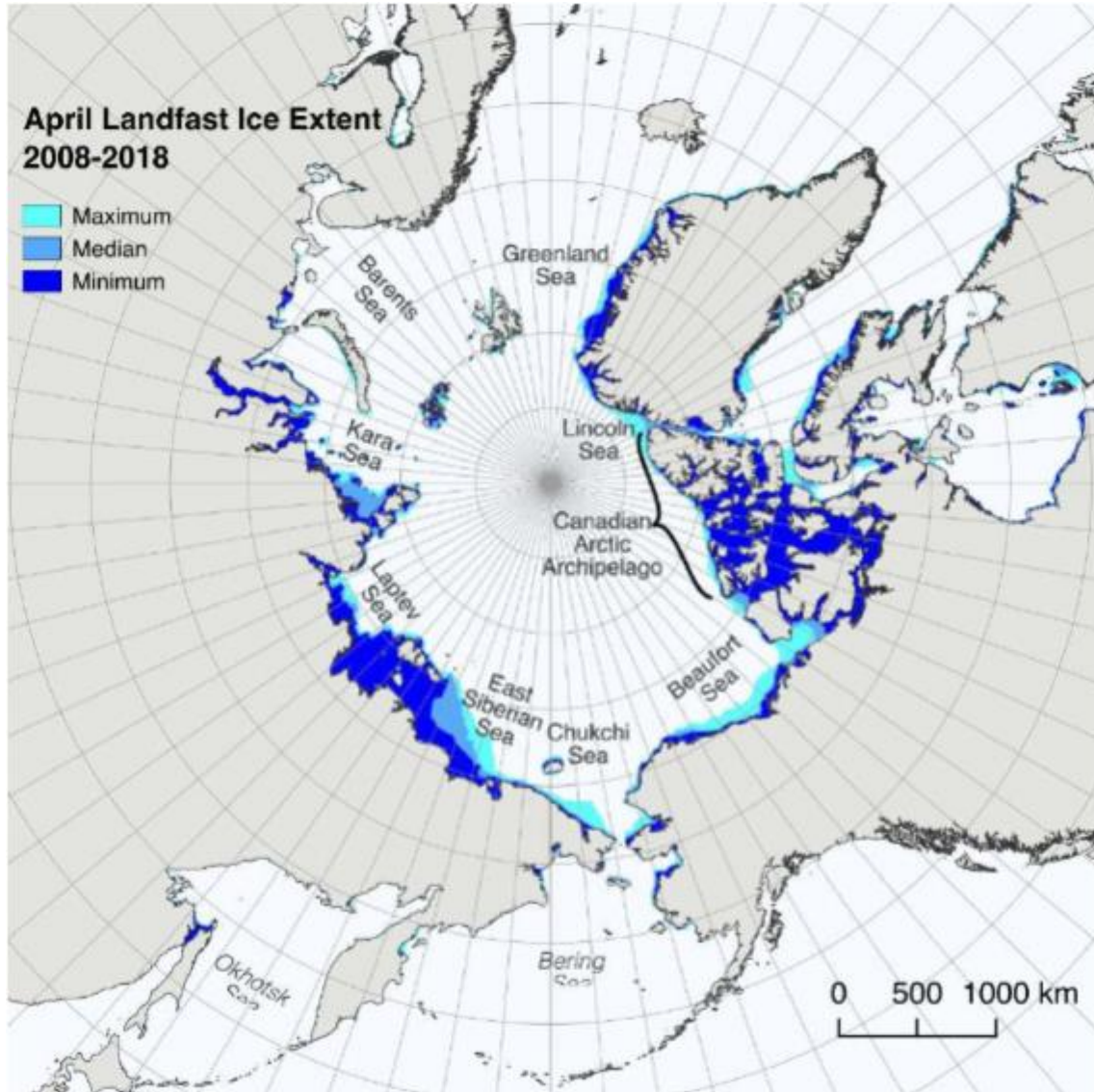
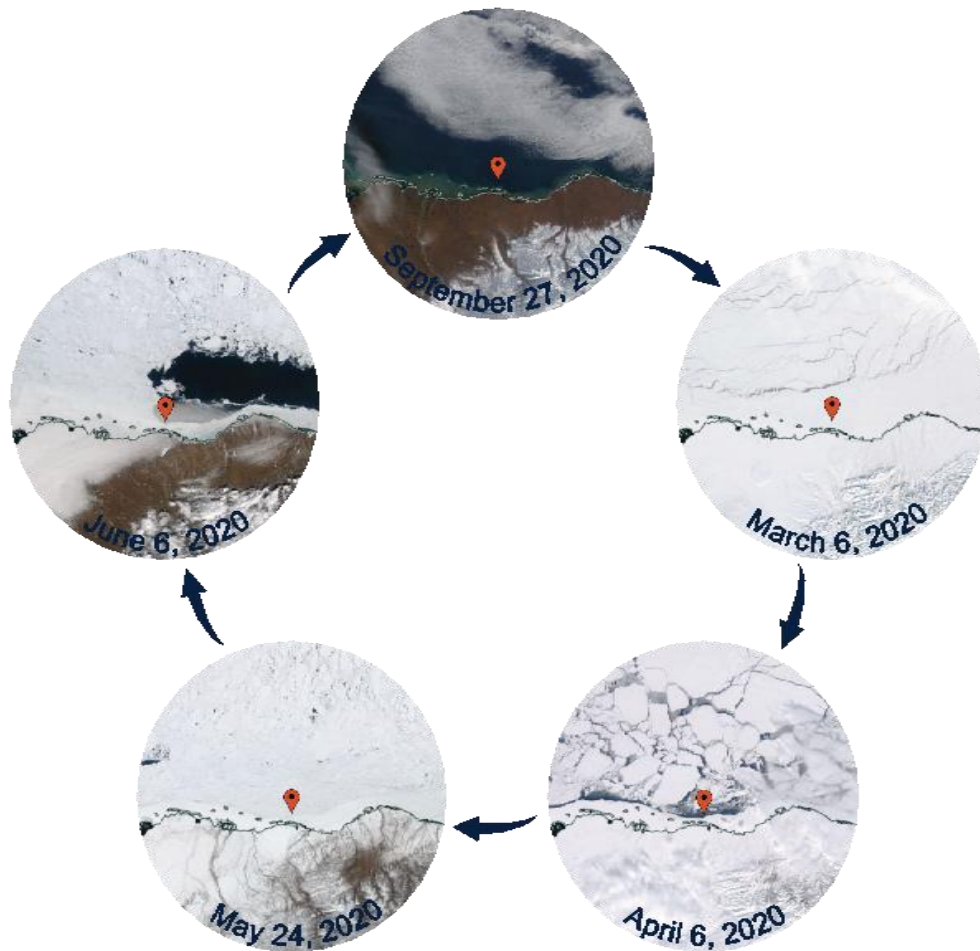


Figure 10. Landfast sea ice presence in the Arctic during the month of April in each year from 2008-2018 (Mahoney, 2018).

### 2.2.1. Growth and breakup cycle

While landfast sea ice can last through the summer in the Canadian Arctic Archipelago and sometimes the Taymyr Peninsula region of Siberia, typically it follows a yearly cycle of formation and breakup. Figure 11 demonstrates this cycle on the Alaskan Arctic coast throughout 2020. In the month of September there is no ice (only clouds are visible over the ocean). By March, landfast sea ice lines the coast and pack ice drifts at its edge. During the winter months, the landfast sea ice forms through a dynamic process.



*Figure 11. Landfast sea ice's annual formation and breakup cycle through NASA Worldview satellite images of the Alaskan Arctic coastline. The coast is outlined in gray. Images from (NASA Worldview, 2023).*

The ice begins as tiny needle-like ice crystals, called frazil, that form as the ocean water begins to freeze. The ice crystals accumulate and bind together, giving the sea surface a greasy appearance. In calm seas, the grease ice develops into thin smooth ice sheets, called nilas, eventually growing into stable ice sheets which gradually thicken. In rough seas, the frazil crystals accumulate into slushy circular disks, referred to as pancakes due to their shape (NSIDC, n.d.). Raised ridges form on the perimeters of the pancakes from the ocean waves bumping the floes into one another. In strong enough waves, pancakes raft over each other, eventually cementing together into an ice sheet with uneven surfaces (Squire, 2020). Sheet ice continues to grow throughout the winter (Squire, 2020). Beginning in shallow waters, pack ice, including nilas and pancake ice, starts to pile up, thickening the landfast sea ice and extending along or away from coastlines (Mahoney, 2018). As the ice piles up, substantial ridges begin to form above and below the surface from the pressure (Figure 12). The pressure ridges can grow deep enough to fasten to the sea floor, becoming bottom-fast (Mahoney, 2018).



*Figure 12. Hunters standing on a pressure ridge (ivu, Iñupiat term) that formed in landfast sea ice (Brewster, n.d.).*

In the spring, the ice begins to break up (Figure 11). Two processes contribute to landfast sea ice breakup. The first is the mechanical process of weakening and erosion from wind and oceanic forces. For this type of breakup to occur, strong offshore winds tend to be present, showing the importance of atmospheric forces (Petrich et al., 2012). Intense seas can pummel the seaward edge into a slurry and the stress of repeated bending of the ice sheet from waves can fracture the ice (Squire, 2007). Anecdotally, these incoming waves cause the ice to break up in strips. A fracture line develops a few tens of meters back from and parallel to the seaward ice edge and the section of ice floats free. This process repeats until the ice sheet is gone. The width of the ice strips is highly dependent on the ice thickness and remains remarkably consistent (Squire et al., 1995). The second breakup process is thermodynamic in nature. Solar radiation incident on the upper surface of the ice causes it to melt, forming melt ponds which are often bright blue. Below these melt ponds, the ice melts at a faster rate than the raised ice around it due to the lower albedo of liquid water to snow covered ice (Figure 13). Thermal breakup can also be enhanced by warm water from below. The timing of thermal breakup correlates with the amount of downwelling solar radiation that is measured in June and July (Petrich et al., 2012).

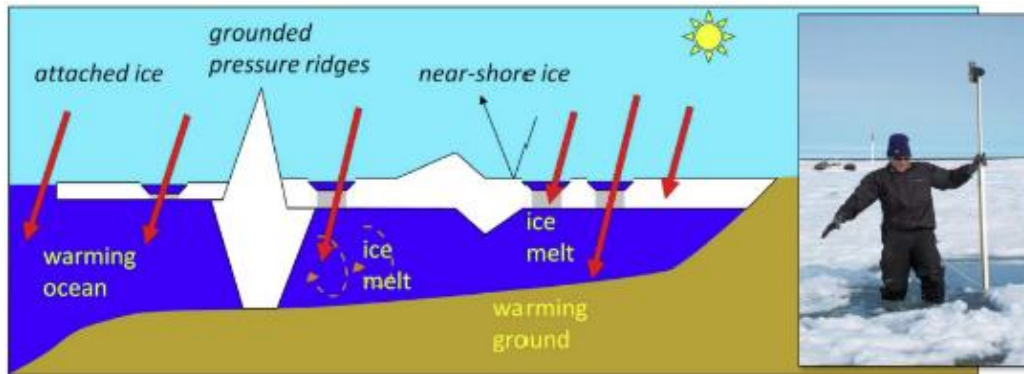


Figure 13. Cross sectional schematic of landfast sea ice during the melt season. Thick arrows represent direct and indirect ice melt from solar radiation. The photo insert, taken June 15, 2009 along the Chukchi Sea coast at Utqiagvik (Barrow), Alaska, demonstrates the preferential melt under melt ponds (Petrich et al., 2012).

While—in reality—break up of landfast sea ice involves both dynamic and thermodynamic processes, the geometry of the coastline can affect which breakup process dominates. In landlocked areas, such as the Canadian Arctic Archipelago, thermodynamic breakup is the predominant process, leading to a consistent breakup date each year. Along open coastlines with landfast sea ice that is not heavily grounded to the bottom, breakup correlates with the cumulative amount of solar energy reaching the ice. When landfast sea ice is heavily grounded, dynamical processes, such as strong winds and currents or changes in local sea level typically control the breakup. Additionally, spring discharge of rivers can mechanically trigger break up near major rivers (Mahoney, 2018).

Landfast sea ice in the Arctic is decreasing in every dimension. With locational dependence, decadal observations indicate landfast sea ice thickness, extent, and duration have decreased (Cooley & Ryan, 2024; Mahoney, 2018; Mahoney et al., 2014). In the channels and straits of the Canadian Arctic Archipelago, which account for almost a third of the total Arctic landfast ice extent of 540,000 km<sup>2</sup>, the maximum annual ice thickness has reduced by approximately ten percent or about 25 cm (Mahoney, 2018). Near Utqiagvik (Barrow), Alaska, a 16-year record indicates the annual maximum thickness decreased by 30 cm from 2000 to 2018 (Mahoney, 2018). Evidence from comparing landfast sea ice extents from 1996 to 2008 to extents from 1973 to 1976 shows that the extent of the seaward edge of landfast sea ice in the late winter of the Chukchi Sea has reduced by 13 km on average in the four decades before 2014. The same study found no change in the landfast sea ice extent in the Beaufort Sea, speculating that the Chukchi Sea had more recurring grounded ice features in the 1970s, leading to this discrepancy (Mahoney et al., 2014). Nonetheless, the annual duration of landfast sea ice has decreased in both seas. Landfast sea ice seasons from 1996-2008 were about 53 days (~2d/yr) shorter in the western Beaufort Sea as compared to the 1973-77 seasons. In the Chukchi Sea, the landfast sea ice season was 38 days shorter (~1.4d/yr) (Mahoney, 2018). A recent study on landfast sea ice breakup over 2000-2022 corroborates the loss of ice days. A statistically significant trend towards earlier breakup was demonstrated with a slope of -7.4 days/decade (Cooley & Ryan, 2024). The study predicts the duration of landfast sea ice will decrease by 9.5 days per 1°C of global warming

above pre-industrial levels – 14.2 days at 1.5°C, and 18.9 days at 2°C across Alaska. However, loss of ice projected at specific communities varies with latitude, with the northernmost community, Utqiagvik, projected to lose 52 days of ice at 2°C of global warming (Figure 14) (Cooley & Ryan, 2024).

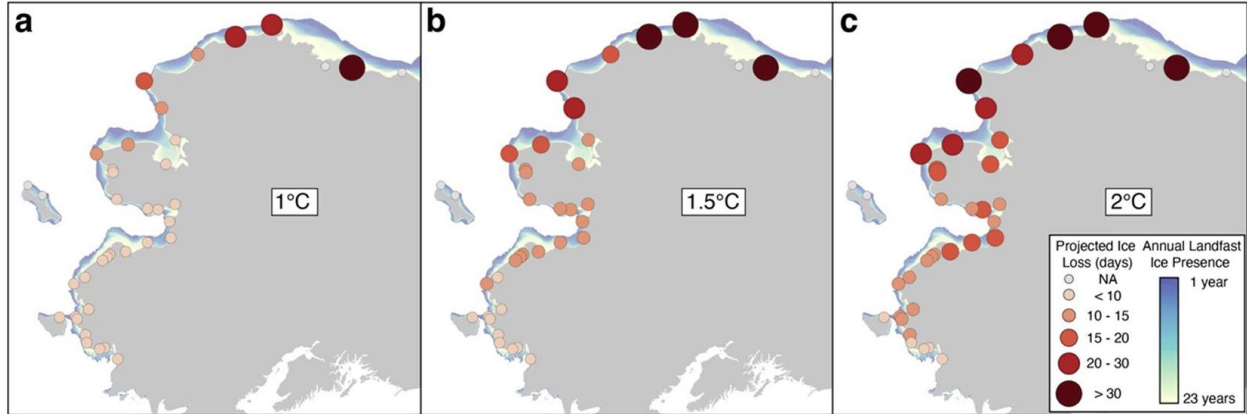


Figure 14. Estimated ice days lost at 38 Alaskan communities for 1°C, 1.5°C, and 2°C of global warming above pre-industrial levels (Cooley & Ryan, 2024).

## 2.3. Wave-ice interactions

Wave-ice interactions encompass more than just the mechanical breakup of sea ice by waves as discussed earlier. Sea ice affects the growth, strength, and propagation of waves. Waves simultaneously affect the formation, strength, breakup, size, and location of sea ice. Waves and ice interact in many complex processes that influence the state of the Arctic. The following subsections focus on two of the most relevant interactions for this work: wave growth in sea ice and wave attenuation by sea ice.

### 2.3.1. Wave growth in sea ice

In contrast to the open waters described in Section 2.1.2, ocean waves can also grow in the presence of discontinuous ice. With the added obstacle of ice in the Arctic, fetches become limited by the ice cover, where the wave growth is a result of the new “effective fetch” (Thomson & Rogers, 2014). With the presence of flaw leads, hard ice edges of landfast sea ice limit fetches in a conventional manner (Figure 15), while floes in partially ice covered zones create many very short effective fetches (Cooper et al., 2022; Smith & Thomson, 2016a). Because of this, waves in ice-infested seas are in a lower frequency range than waves generated in open water; they need very long durations to grow (Squire, 2007).

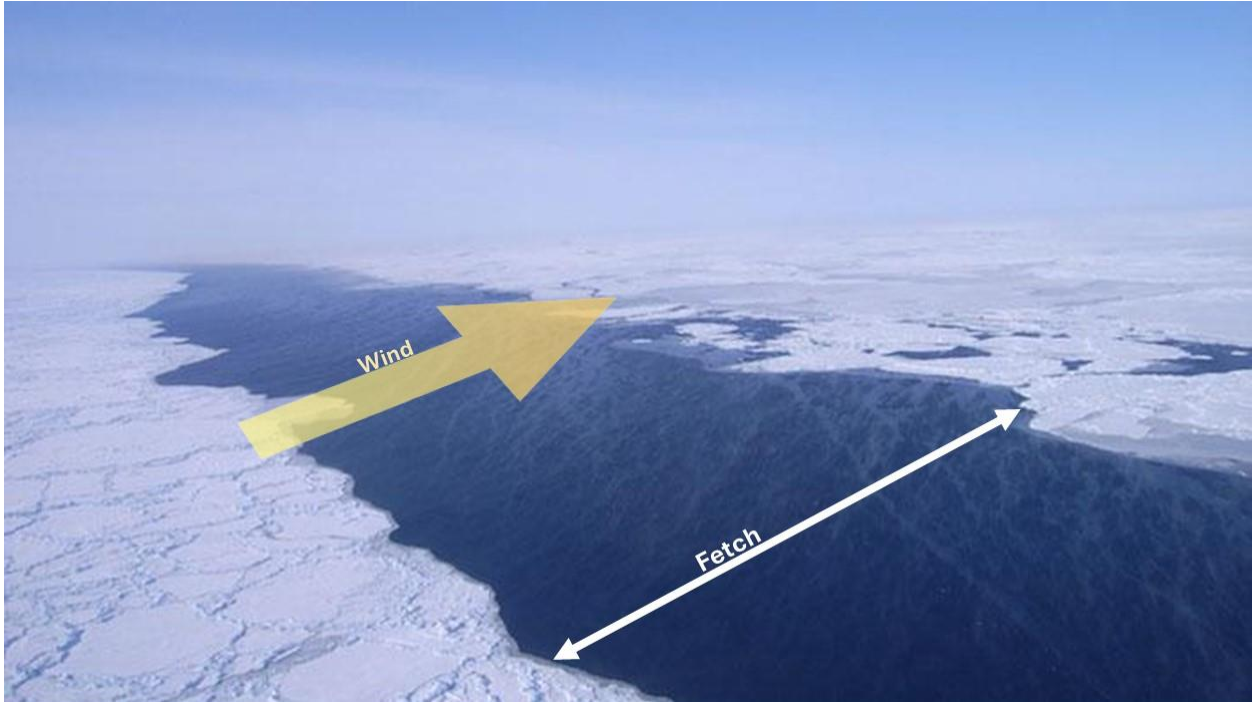


Figure 15. Landfast sea ice (left) and drifting pack ice (right) bound a flaw lead off the coast of Utqiagvik (Barrow), Alaska (Open Lead | Project Jukebox, n.d.). The ice on either side limits the effective fetch to the width of the flaw lead, increasing the likelihood of fetch-limited wave generation. If the wind is directed as portrayed, the fetch would extend as shown.

The nondimensional Equations 2.1-2.4 can be applied to the effective fetches. Although uniform winds are rarely observed, the nondimensionalized equations are often in agreement with observations (Thomson & Rogers, 2014). Ocean waves are rarely limited purely by distance or purely by the wind, but rather a combination. The likelihood that the ocean behaves in a fetch-limited manner is higher during the beginning of summer when shorter fetches are more prominent with an increased ice extent. A comparison of the nondimensional wave energy,  $\varepsilon$ , versus nondimensional distance,  $\chi$ , from data collected during 2014 demonstrated that for purely distance-limited waves in the Beaufort Sea, the correlation of distance with wave energy is significant.

$$\varepsilon = 1.7 \times 10^{-7} \chi^{0.98} \quad 2.6$$

where coefficients from Equation 2.5 are empirically determined with  $A$  as  $1.7 \times 10^{-7}$  and  $a$  as 0.98 (Figure 16) (Smith & Thomson, 2016a).

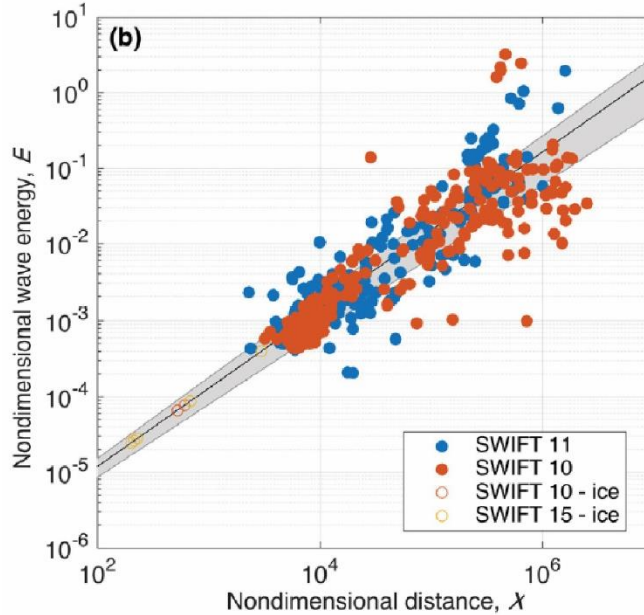


Figure 16. Nondimensional wave energy and distance in the Beaufort Sea of distance-limited waves from open water. The data is fit with a regression slope of  $\chi^{0.98}$  (black line) and associated normalized root-mean-square error (shaded gray region) (Smith & Thomson, 2016a).

### 2.3.2. Wave attenuation by sea ice

While hard ice edges limit fetches in a conventional manner, waves still penetrate into the ice where they are rapidly attenuated (Squire, 2020). Since waves can break up ice while simultaneously being suppressed by the ice, the interactions of waves and ice are complex. Sea ice is compliant, so the ice plate itself deforms as ocean waves pass beneath it. However, too much bending strain on the ice can cause it to weaken and break. In the Arctic, this destructive zone of intense energy loss typically extends 10-20 km while in Antarctica's Southern Ocean, the larger seas impact a much greater zone (Squire, 2020). Along coastlines and particularly in embayments, such as harbors, landfast sea ice can become coupled to the waves that enter and flex the ice, potentially leading the ice to break up (Squire, 2020). While waves penetrating ice have been recorded to travel great distances throughout the Arctic ocean, generally they are rapidly attenuated by ice as energy is lost from the waves (Squire, 2020; Squire et al., 1995).

Generally, attenuation is greater in thicker ice of higher concentrations. The two key mechanisms for attenuation are the scattering and dissipation of wave energy by sea ice (Thomson & Rogers, 2014). Scattering conservatively redistributes energy rather than eliminating it. For scattering, gravity is the most important restoring force (Squire et al., 1995). The most scattering occurs when the orders of ice-length scales and ocean wavelengths are similar. When they are not of similar orders, scattering does not occur. Since pancake ice and frazil slurries have characteristic length scales much smaller than ocean wavelengths, dissipation of the waves through ice breakup occurs as well as through the buildup of the outer edges of pancake ice (Squire, 2020).

Dissipation removes energy from the wave field in a non-conservative process. It eliminates

higher frequency waves before lower frequency ones causing the ice to act as a low pass filter (Squire, 2020). Scattering takes precedence until about 0.1 Hz, when flexural rigidity overwhelms the restoring force of gravity and dissipation takes over (Squire et al., 1995). Dissipative attenuation maintains smaller ice floe sizes (Squire, 2020). As the Arctic wave climate becomes increasingly energetic, extensive pancake ice formation is being observed in the western Arctic (Squire, 2020).

### 2.3.3. Waves in landfast sea ice zones

While work in recent years is rapidly advancing understanding of wave-ice interactions in pack ice, wave-ice interactions in landfast sea ice zones remain understudied. This especially includes the generation of waves in seasonal flow leads and their attenuation in the landfast sea ice. It is not known what fraction of the waves in the seasonal landfast ice zone are limited by fetch vs. duration, and the key atmospheric processes that determine the characteristics of these waves. Analyses here focus on the understudied spring-summer breakup period using seafloor mooring data, modelled atmospheric data, and satellite imagery to investigate how atmospheric conditions influence wave-ice interactions. In the next chapter the datasets are described, and the methodology used to fill this knowledge gap is outlined.

### 3. Methodology

This chapter explains the in-situ data, atmospheric reanalysis, and satellite imagery used, as well as the processing and analysis steps taken to investigate the wave growth in fetch-limited conditions. All of the data processing, except the measurements taken using NASA Worldview described in 3.1.3 Satellite imagery, was performed using Python script in Google Colab<sup>1</sup>, a Jupyter notebook hosted in the Google Suite (Figure 18) (Colab.Google, n.d.).

#### 3.1. Datasets

The data utilized in this analysis originate from three sources: three in-situ moorings, atmospheric reanalysis from ERA5, and satellite imagery from Worldview NASA. The following subsections explain the collection or modeling process for each type, as well as individual data processing that was performed.

##### 3.1.1. Moorings in the Arctic

This study focuses on three moorings positioned as a cross-shore array off Oliktok Point in Prudhoe Bay (Figure 17a) which measured the wave field with increasing distance from the shore. The moorings are numbered with increasing latitude and are referred to as Mooring 1 (the southernmost mooring), Mooring 2 (the middle mooring), and Mooring 3 (the northernmost mooring), as shown in Figure 17. Figure 17b (Thomson & Smith, 2024). All components of the moorings were on the seafloor with approximate depths at these locations of 6, 14, and 20 m, respectively.

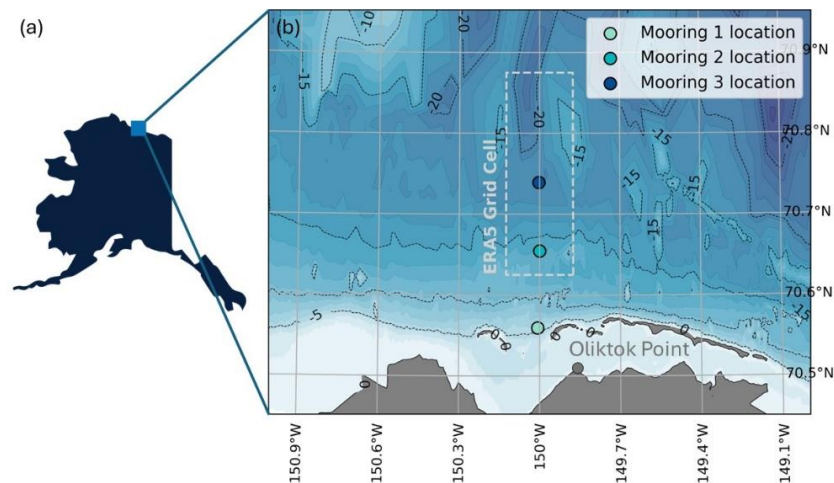


Figure 17. The moorings were deployed (a) near Prudhoe Bay off Oliktok Point on the Northern slope of Alaska. At the test site (b) moorings are positioned in a cross-shore array along the 150°W longitude line. The light gray boxed in area marks the coverage of the grid cell used from ERA5. The ERA5 grid cell includes Moorings 2 and 3 but is offset from Mooring 1.

<sup>1</sup> The code is available at <https://github.com/mcsangillo/arctic-coastal-fetch-analysis.git>.

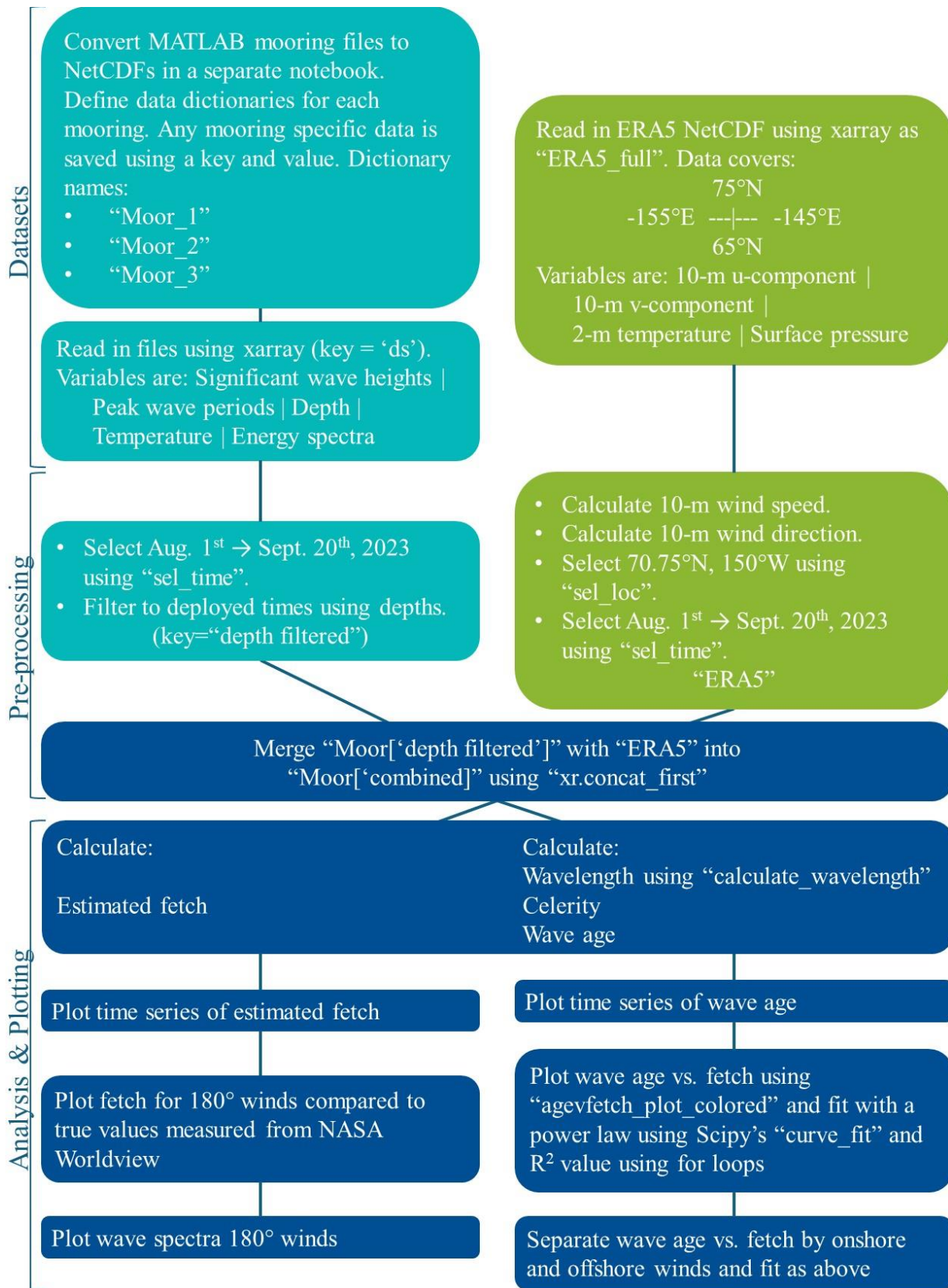


Figure 18. Flow chart outlining the code used for this analysis.

The three seafloor moorings were deployed along the 150°W longitude line between April 18<sup>th</sup>, 2023 and September 20<sup>th</sup>, 2023 and provide a record of the variability of conditions with distance offshore during the landfast sea ice’s annual breakup. Each mooring was equipped with a seafloor pressure and temperature logger, called an RBR, that was secured by chain to anchors on either end (Figure 17Figure 19). To minimize risk to the mooring from sea ice, the moorings did not have surface expressions. Instead, a surface float and retrieval system were attached. The compartment attached to the buoy (yellow) contained line. During retrieval the line was released, allowing the float to rise to the surface. If the float was not released, the retrieving ship had to trawl for the seafloor mooring, which was why so much chain was included to make a larger target.



Figure 19. An example of one of the moorings deployed with labelled components. The buoy (yellow) is released on a tether to the surface for retrieval, while the anchors on either side of the instrument secure it to the seafloor. Image courtesy of Jim Thomson.

The RBR continuously sampled at 2 Hz and recorded hourly. In post-processing, spectral analysis was used to calculate energy from the pressure over 1799 frequencies from  $0.8 \text{ mHz} < f < 1.0 \text{ Hz}$ , however, only the  $0.03 \text{ Hz} < f < 1.0 \text{ Hz}$  range is used in this analysis, as this is the frequency range for wind waves (Figure 4) (Thomson & Smith, 2024). The seafloor pressure spectra were corrected for depth attenuation and converted to surface wave spectra using frequency-dependent depth attenuation given by linear wave theory. Since energy at higher frequencies attenuates with depth at a higher rate, there was noise at higher frequencies for all three moorings. The noise was trimmed at a depth-dependent cutoff, and each spectrum was extrapolated to the highest frequency of 1.0 Hz using a canonical  $f^{-4}$  form. Energy in this frequency region is preferentially reduced by the attenuation in sea ice which makes the canonical form  $f^{-4}$  an upper bound on the energy. The cutoff frequencies for each mooring are listed in Table 1. From the integral of the energy spectra, the significant wave heights were determined, and peak wave periods were determined from the frequencies of the peak energies of the energy spectra (Hošeková et al., 2021). The depths and energy spectra were also included in this original dataset. Additional quality control was performed once receiving the dataset to filter for large changes in depth. Any data with depths less than the depth cutoffs listed in Table 1 were removed. For Mooring 1 this removed data for the first three weeks of June when the mooring appears to have been disturbed, as well as during deployment and recovery. For Moorings 2 and 3 the depth filtering only removed data during deployment and recovery.

Table 1. Numerical information for each mooring.

	<b>Mooring 1</b>	<b>Mooring 2</b>	<b>Mooring 3</b>
<b>Location</b>	70.5594°N, 150.0071°W	70.6546°N, 150.0001°W	70.7394°N, 150.003°W
<b>Average depth</b>	6.12 m	13.82 m	19.55 m
<b>Depth-dependent frequency cutoff</b>	0.35 Hz	0.23 Hz	0.19 Hz
<b>Depth cutoff</b>	5.57 m	13m	19 m

### 3.1.2. Atmospheric reanalysis

Estimates of wind parameters from the atmospheric and wave reanalysis dataset ERA5 are used with mooring observations to estimate fetch and wave age (Hersbach et al., 2023). ERA5 provides global estimates of many atmospheric, land, and oceanic climate variables by combining historical and current observations through advanced modelling and data assimilation systems (Setchell, 2020). Produced by the Copernicus Climate Change Service at the European Centre for Medium-Range Weather Forecasts (ECMWF), ERA5 is the fifth generation of ECMWF atmospheric reanalysis of global climate. Updated daily with a latency of five days, it provides hourly estimates from January 1940 to the present at 0.25° grid cell resolution (~31 km) for atmospheric variables (Hersbach et al., 2023; Setchell, 2020). The grid cell that was closest to the moorings was centered at 70.75°N, 150°W and covered from 70.625°N to 70.875°N and 150.125°W to 149.875°W, as shown in Figure 17.

Four variables were retrieved from ERA5 for the duration of the moorings' deployment: 10-m  $u$ -component of wind (m/s), 10-m  $v$ -component of wind (m/s), 2-m air temperature (K), and surface pressure (Pa). The 10-m  $u$ - and  $v$ -components of wind are the eastward and northward components of the horizontal movement of air at a height ten meters above the surface of the Earth, respectively. They were used with the tangent to calculate the scalar wind speed ( $U$ ) in m/s and wind direction ( $wdir$ ) in degrees clockwise from North. 2-m temperature is the temperature of the air at a height two meters above the surface of the land, sea, or inland waters. It was converted to degrees Celsius by subtracting 273.15°. Surface pressure is a measure of the weight of all the air in a column vertically above a point on the Earth's surface as force per unit area. It was converted to kilopascals by dividing by 1000.

### 3.1.3. Satellite imagery

Satellite imagery from NASA's Worldview product was also used to develop a visual understanding of the sea ice conditions and take distance measurements relevant to fetch analysis (NASA Worldview, 2023). The ability to use this optical imagery to provide an understanding of the ice progression throughout the full observational period was limited by cloud cover, but some clear sky images were used (e.g., Figure 20). The measuring tool built into NASA Worldview

was used as originally intended, as well as to build straight lines to measure against (NASA Worldview, 2023). An example of this method is shown in Figure 20. A similar method was also used to calculate the angles that split onshore versus offshore winds. Onshore winds are winds that blow onto land while offshore winds are winds that blow off land.

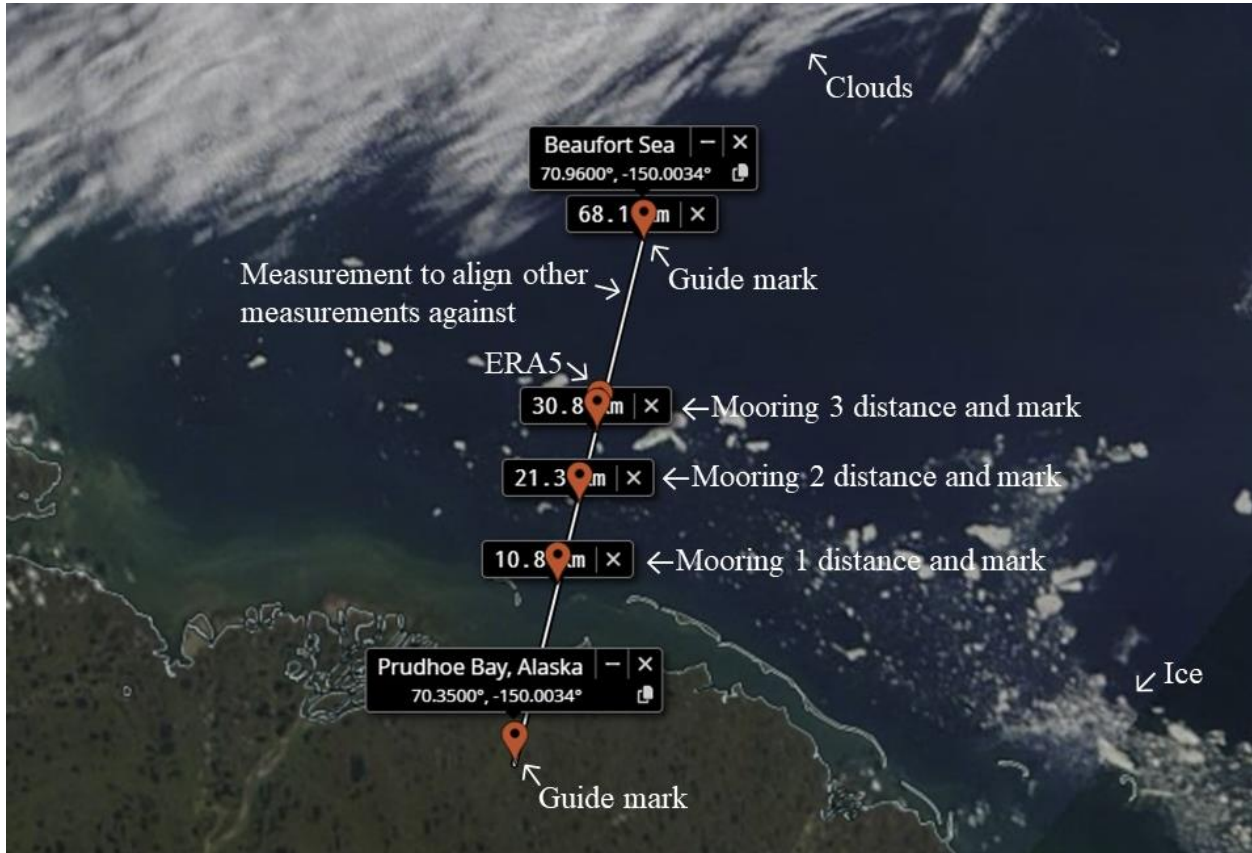


Figure 20. The satellite image on Aug. 20<sup>th</sup>, 2023 from NASA Worldview demonstrates how the measuring tool was used to measure distance from shore and as an alignment tool (NASA Worldview, 2023). Some remnant ice is visible over and to the east of the moorings, limiting wave growth.

## 3.2. Derived parameters

The following two subsections describe how two parameters—the inferred fetch and wave age—were derived by combining the mooring data and ERA5 reanalysis data.

### 3.2.1. Empirical fetch calculations

The inferred fetch length was estimated from the power law and definitions of nondimensional variables described in 2.1.3 Duration and fetch-limited waves based on observed wave heights and estimated wind speeds. Reorganizing Equations 2.1, 2.3, and 2.6,

$$x = \sqrt[a]{\frac{g^{-(a-2)} H_s^2 U^{2a-4}}{16A}}, \quad 3.1$$

where  $A = 1.7 \times 10^{-7}$  and  $a = 0.98$  and converted to kilometers (Smith & Thomson, 2016b).

### 3.2.2. Wave age calculations

Wave age was used to quantify the relative development of the waves. By dividing the wave celerity—or wave speed—by the wind speed, the nondimensional quantity of wave age describes the wave development with respect to the wind supplied. Calculation of two preliminary variables was necessary to derive the wave age: the wavelength ( $L$ ) in m and the wave celerity ( $C$ ) in m/s. The wavelength was determined iteratively using the equation from linear wave theory in transitional water depths by

$$L = \frac{gT_p^2}{2\pi} \tanh\left(\frac{2\pi d}{L}\right), \quad 3.2$$

where  $T_p$  is the peak wave period and  $d$  is the water depth (U.S. Navy Corps of Engineers, 2008). Since the conditions observed by the moorings did not fully fall into shallow-water or deep-water based on the length of waves relative to the depth, it was necessary to use this full equation. The wave celerity is related to the wavelength by

$$C = \frac{L}{T_p} \quad 3.3$$

(U.S. Navy Corps of Engineers, 2008). From the wave celerity and windspeed, the wave age is calculated as

$$\text{Wave age} = \frac{C}{U}, \quad 3.4$$

and is often referred to as wave age or  $C/U$  (Thomson & Rogers, 2014).

### 3.3. Data analysis

Three steps were taken in order to investigate how the spatial variation of fetches affects the development of waves in the coastal Arctic.

1. Specific fetch conditions and their wave spectra were investigated in order to verify fetch-limited wave growth. Instances of directly offshore winds correspond with fetches

limited to the mooring's distance from shore. The wave spectra of such instances were analyzed for fetch-limited characteristics.

2. For each mooring the wave age was plotted against the estimated fetch for the mooring's entire dataset. The data was split into data during onshore winds and data during offshore winds and inspected separately.
3. The wave age versus estimated fetch plots for each mooring were compared to each other to observe trends corresponding to distance from shore.

The results from these three steps are explained in the subsequent chapter.

## 4. Results

This chapter explains the results of the steps described in 3.3 Data analysis that were taken in order to investigate how the spatial variation of fetches affects the development of waves in the coastal Arctic. Fetches are a result of both the distance from land and the changing distance to the ice edge. This chapter details how:

1. Fetch-limited wave growth exhibits certain characteristics that are identified in offshore wind conditions and their wave spectra.
2. The wave age follows a power law trend with the inferred fetch, with onshore wind conditions fitting the power law more closely.
3. And, the wave age also trends upwards with increasing distance from shore.

These results are described in detail in the following.

### 4.1. Summary of observed wave and atmospheric conditions

Significant wave heights, peak wave periods, and atmospheric conditions at the mooring locations (Figure 17) are shown in Figure 21. The significant wave heights typically increase with distance from shore from Mooring 1 to Mooring 3 (Figure 21a). The time series of significant wave heights and peak wave periods from Aug. 1<sup>st</sup> to Sept. 20<sup>th</sup>, 2023, show an increase in wave activity on Aug. 23<sup>rd</sup> (Figure 21). The time series of ERA5 variables also demonstrate a growing wind from the west, decreasing air temperature, and increasing surface pressure. By this time the landfast sea ice has receded and sparse sea ice remains (from NASA Worldview imagery of Aug. 20<sup>th</sup>). Thus, the increase in wave activity likely corresponds with the advection of remaining sea ice away from the area increasing the effective fetch. The significant wave heights, peak wave periods, wind speed, and wind direction are used for further analysis. While the air temperature and surface pressure are not included in further analysis, they are included here for a more complete description of the atmospheric conditions and could be used in future work.

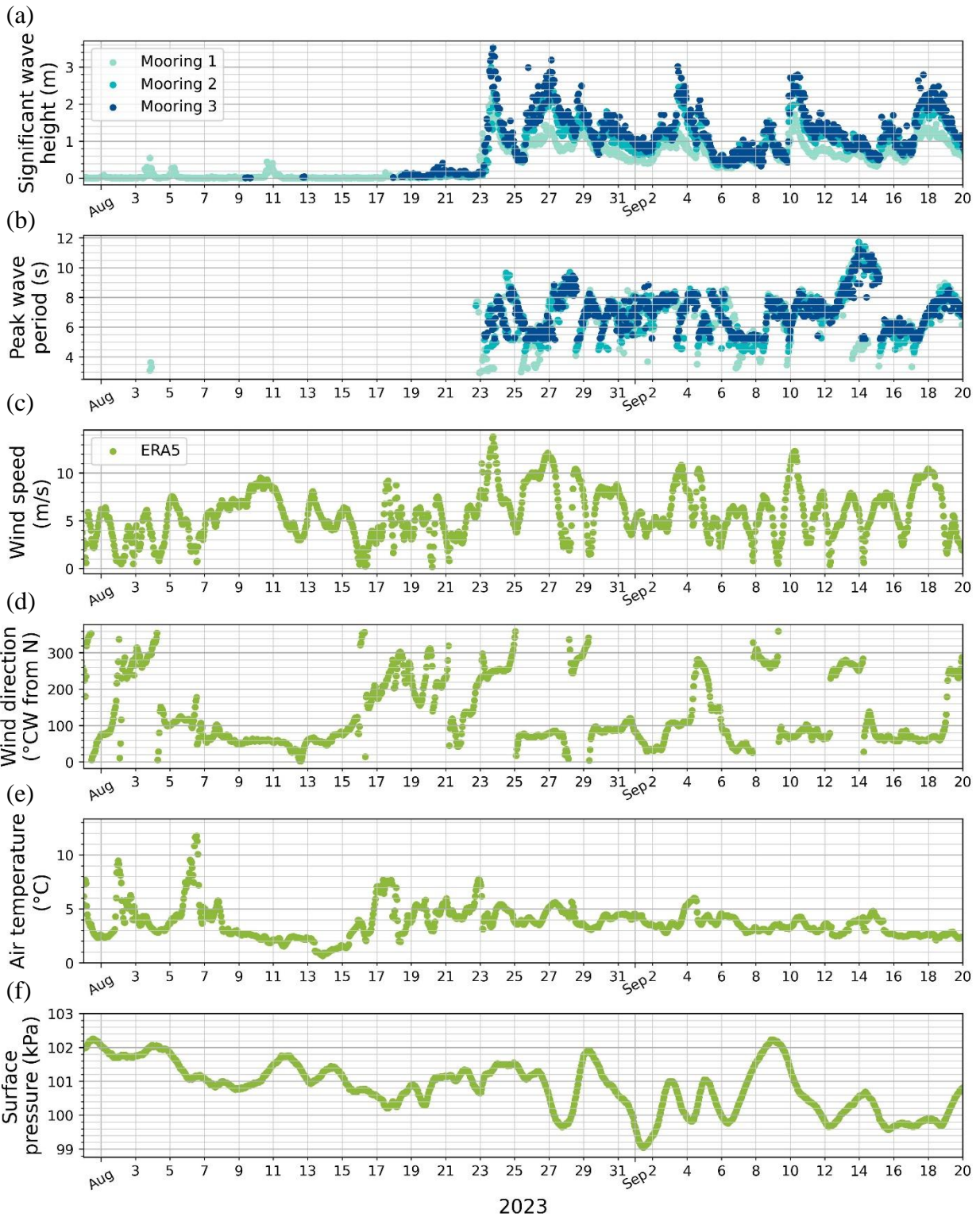


Figure 21. Time series of the mooring (a & b) and ERA5 (c, d, e, & f) data from Aug. 1<sup>st</sup> to Sept. 20<sup>th</sup>, 2023. (a) Significant wave heights appear to increase from Mooring 1 to Mooring 3. (b) Since high frequency waves are attenuated with depth, the peak wave periods are cut off at low periods.

## 4.2. Fetch

The time series of the estimated fetch, as described by 3.2.1 Empirical fetch calculations, shows fetch estimates for Moorings 2 and 3 beginning on Aug. 18<sup>th</sup>, 2023, while Mooring 1 estimated begin shortly after deployment (Figure 22). The estimated fetch oscillates until it increases from the meter scale to the 100 km scale on Aug. 23<sup>rd</sup> and continues to fluctuate around 100 km from Aug. 24<sup>th</sup> until the end of the dataset (Figure 22).

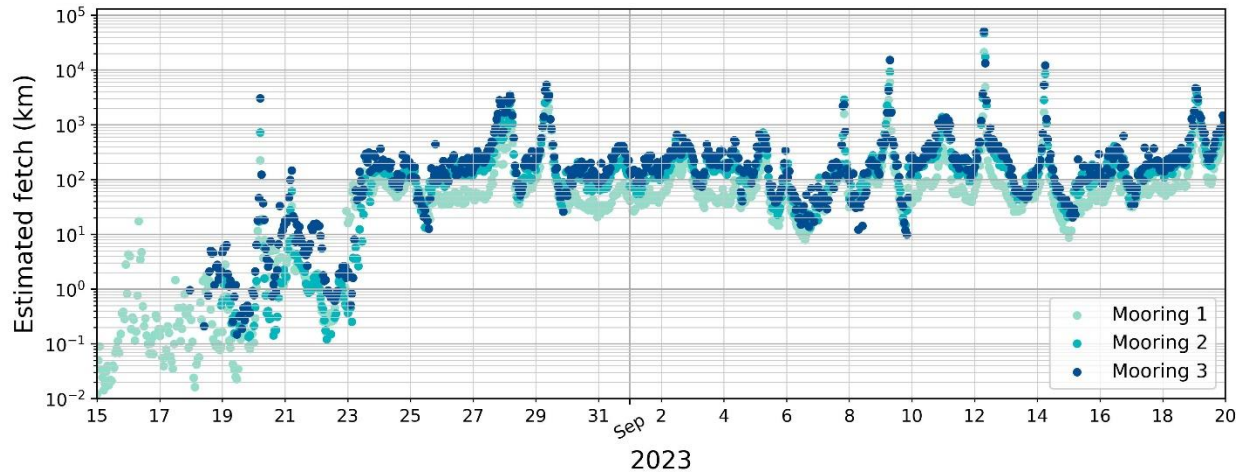


Figure 22. Time series of the estimated fetch from Aug. 15<sup>th</sup> to Sept. 20<sup>th</sup>, 2023. The fetch appears to increase from Mooring 1 (light green) to Mooring 3 (blue).

### 4.2.1. Fetch-limited growth from the coast

Examining offshore wind conditions enable understanding whether observations follow more canonical fetch-limited growth. During directly offshore wind conditions, the fetch is limited by the shore on its windward edge and the mooring location on its leeward edge. Thus the fetch is equal to the mooring's distance from shore (Figure 23). From NASA Worldview, the offshore distances for Moorings 1, 2, and 3 during directly northward (180°) wind conditions are 10.8 km, 21.3 km, and 30.8 km, respectively. Limiting the wind direction from 175° to 185°, four instances for all three moorings occur (Figure 24). The first instance follows the expected conditions of increasing fetch from Mooring 1 to Mooring 3 and fetches shorter than or equal to the physically limiting distance from shore. The three other instances do not follow the expected conditions. During the second instance, the moorings are in an unexpected order, and during the third and fourth instances, the estimated fetches are greater than the physically limiting distance from shore. This is potential due to the nature of an instance. None of these instances are consecutive, so the discrepancies could be from residual waves from other wind directions with different fetches.

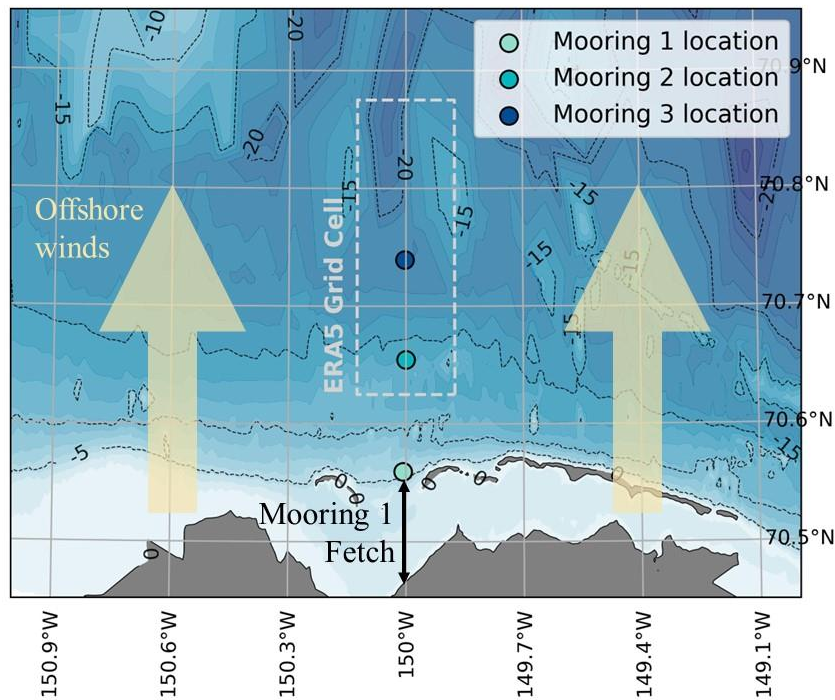


Figure 23. During directly offshore winds, the fetch is limited by the distance from shore. The fetch for Mooring 1 is included to demonstrate this.

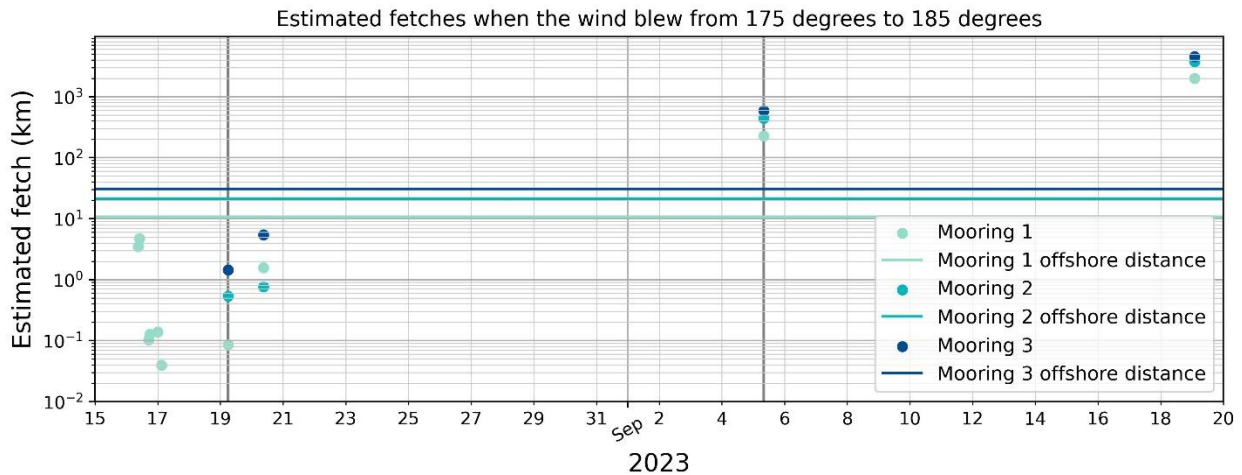


Figure 24. There are four instances where all three moorings have estimated fetches and simultaneously the wind blows directly offshore ( $175^\circ < wdir < 185^\circ$ ). The gray vertical lines mark the two instances that are used for further analysis in Figure 25. Discrepancies in the order of the moorings and estimated fetches that are longer than the physically allowable fetches, could be due to residual waves from other wind directions. However, the spacing between moorings remains consistent, not including the second instance, with Mooring 1 being spaced further from Mooring 2 than Mooring 2 from Mooring 3.

Inspecting the retained instances further, the wave spectra of Aug. 19<sup>th</sup> at 6 AM and Sept. 5<sup>th</sup> at 8 AM show more energy concentrated at higher frequencies. For both instances the average slope towards the peak energy at lower energies is steeper than the average slope away from the peak energy at higher at higher frequencies (Figure 25). In addition, the peak energy increases from Mooring 1 to Mooring 3. The double peaks that occur in some of the spectra could be from residual waves from other wind directions that would correspond with different fetches.

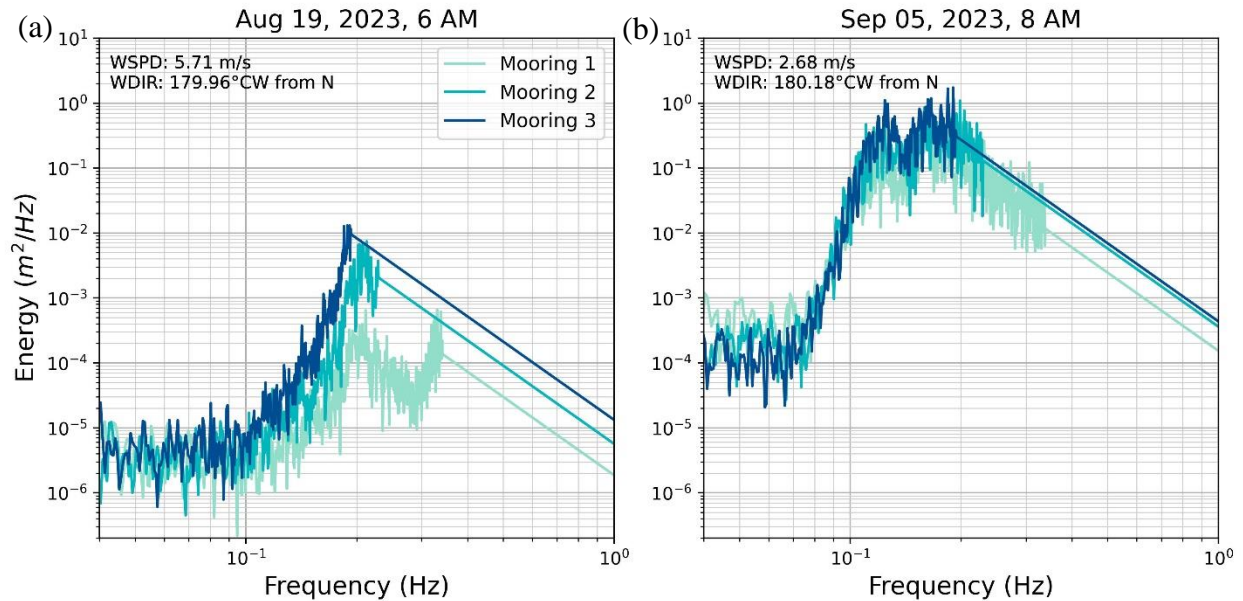


Figure 25. The wave spectra of the identified instances of directly offshore winds from Figure 24. The energy is extrapolated at high frequencies as described by 3.1.1 Moorings in the Arctic. More energy is concentrated at higher frequencies, which correspond to less developed waves. The peak energies also increase with increasing fetch (from Mooring 1 to Mooring 3).

The fetch and wave spectra for fetches limited by the mooring’s distance offshore show consistent spacing between moorings, more energy at higher frequencies, and increasing peak energy from Mooring 1 to Mooring 3, which indicate fetch-limited wave growth between locations.

### 4.3. Wave age

The time series of wave age, as described by 3.2.2 Wave age calculations, from Aug. 15<sup>th</sup> to Sept. 20<sup>th</sup>, 2023, show the development of waves with time. Wave ages below one correspond to younger, less developed waves where the wind is faster than the waves. Wave ages above one correspond to older, more developed waves where the waves are faster than the wind. Since wave ages are dependent on the significant wave heights, peak wave periods, and depth of the moorings, wave age is limited to times where all three variables have values. Thus, wave ages begin to show on Aug. 22<sup>nd</sup>. This is the day before the wave activity increases, and wave ages remain relatively low during this time. Commonly below one, the wave ages peak during events and are generally greater at further offshore moorings.

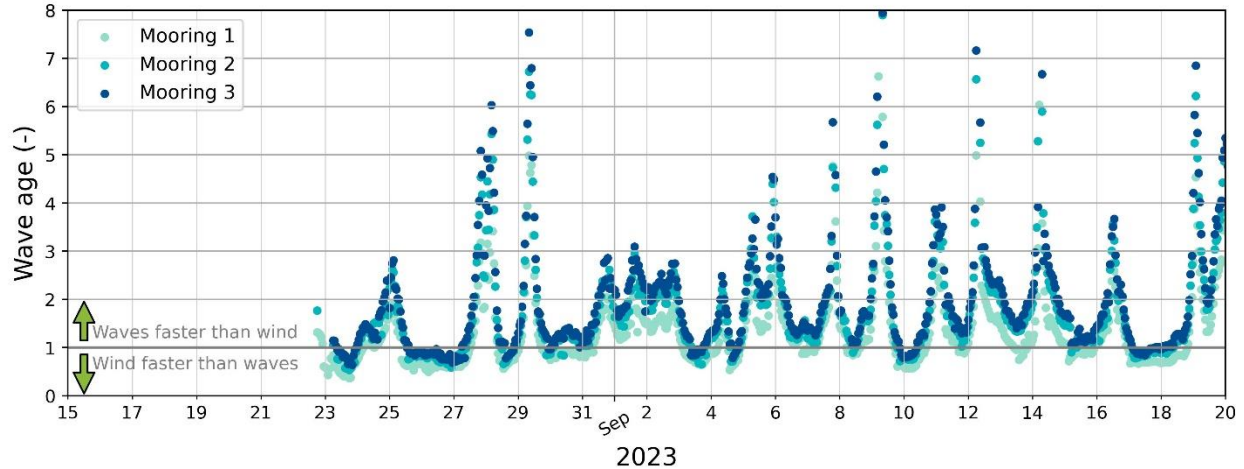


Figure 26. Time series of the wave age from Aug. 15<sup>th</sup> to Sept. 20<sup>th</sup>, 2023.

#### 4.3.1. Onshore and offshore winds

Wave age is expected to increase with fetch, as there are longer distances for waves to develop under the transfer of energy and momentum from the wind to the ocean surface. Fetches during offshore winds are generally shorter than fetches during onshore winds, as they are limited by coastlines. Investigating this wind direction dependence, Figure 27, Figure 28, and Figure 29 demonstrate the correlation between the wave age and the estimated fetch on log-log plots for Mooring 1, Mooring 2, and Mooring 3, respectively. Figure 27a, Figure 28a, and Figure 29a include and fit all of the data from their respective moorings. They show that the wave age increases with the estimated fetch by a power law. The data were fit using `curve_fit` from Scipy, and have the same exponent ( $a$ ), meaning the wave age of each mooring increases with the same rate on a log-log plot, but starts at a different wave age (Table 2).

Table 2. Table of power law constants ( $A$  &  $a$ ) and  $R^2$  values for the full dataset, onshore category, and offshore category for each mooring.

$y = Ax^a$		Mooring 1	Mooring 2	Mooring 3
$A$	Full	0.15	0.14	0.13
	Offshore	0.18	0.21	0.18
	Onshore	0.15	0.13	0.12
$a$	Full	0.49	0.49	0.49
	Offshore	0.46	0.42	0.45
	Onshore	0.49	0.5	0.5
$R^2$	Full	0.83	0.8	0.77
	Offshore	0.7	0.72	0.65
	Onshore	0.87	0.83	0.81

In Figure 27b, Figure 28b, and Figure 29b, the data is categorized into onshore winds and offshore winds. Each category is separately fitted and plotted together. Both onshore and offshore winds follow the power law, with onshore winds tending towards similar power laws to the entire datasets and offshore winds fitting steeper slopes in the log-log plots.

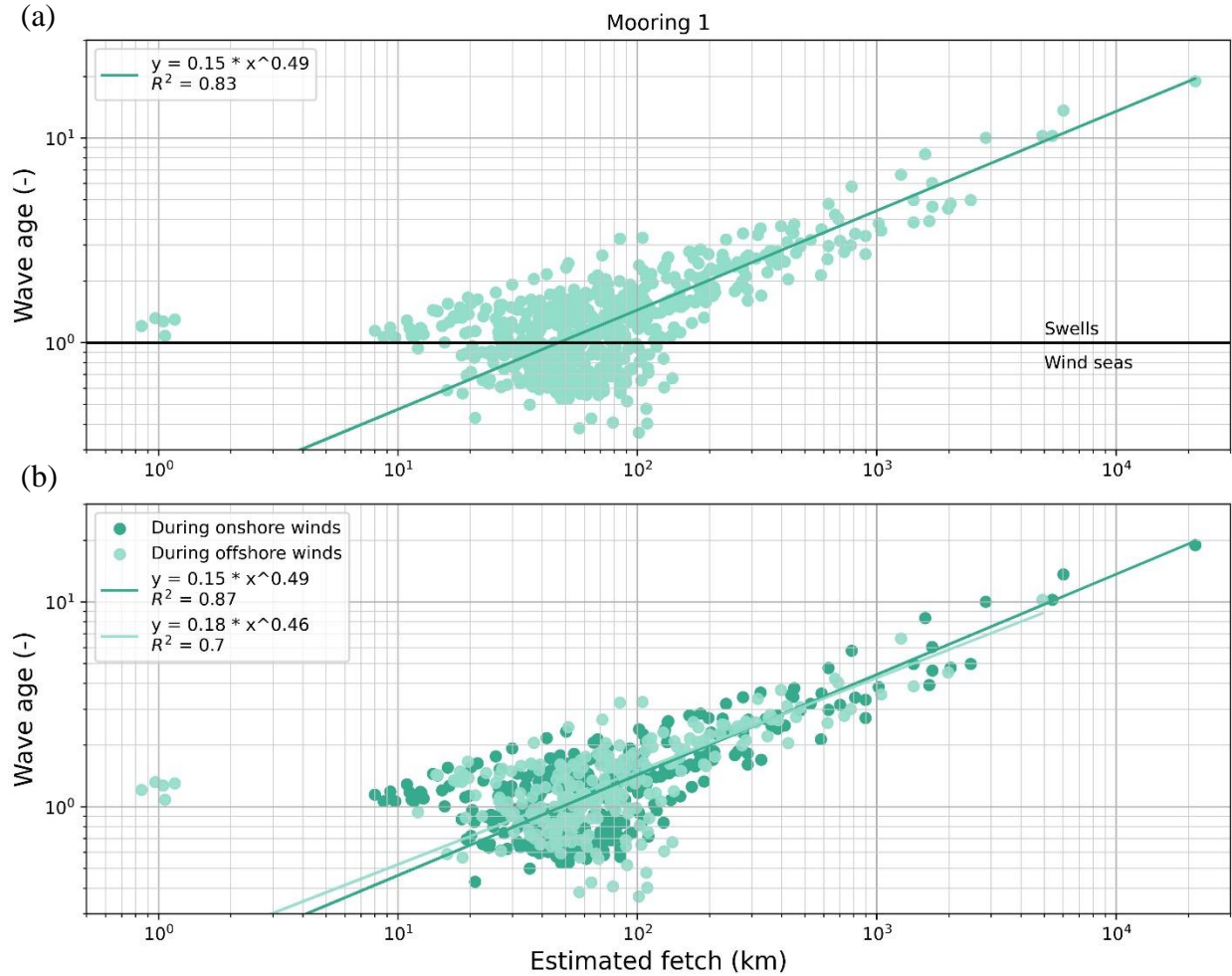


Figure 27. The wave age plotted with estimated fetch and fit with a power law relation for Mooring 1. (a) describes all of Mooring 1's data while (b) categorizes the data by wind direction and fits them separately. Onshore winds demonstrate the best power law fit with an  $R^2$  value of 0.87.

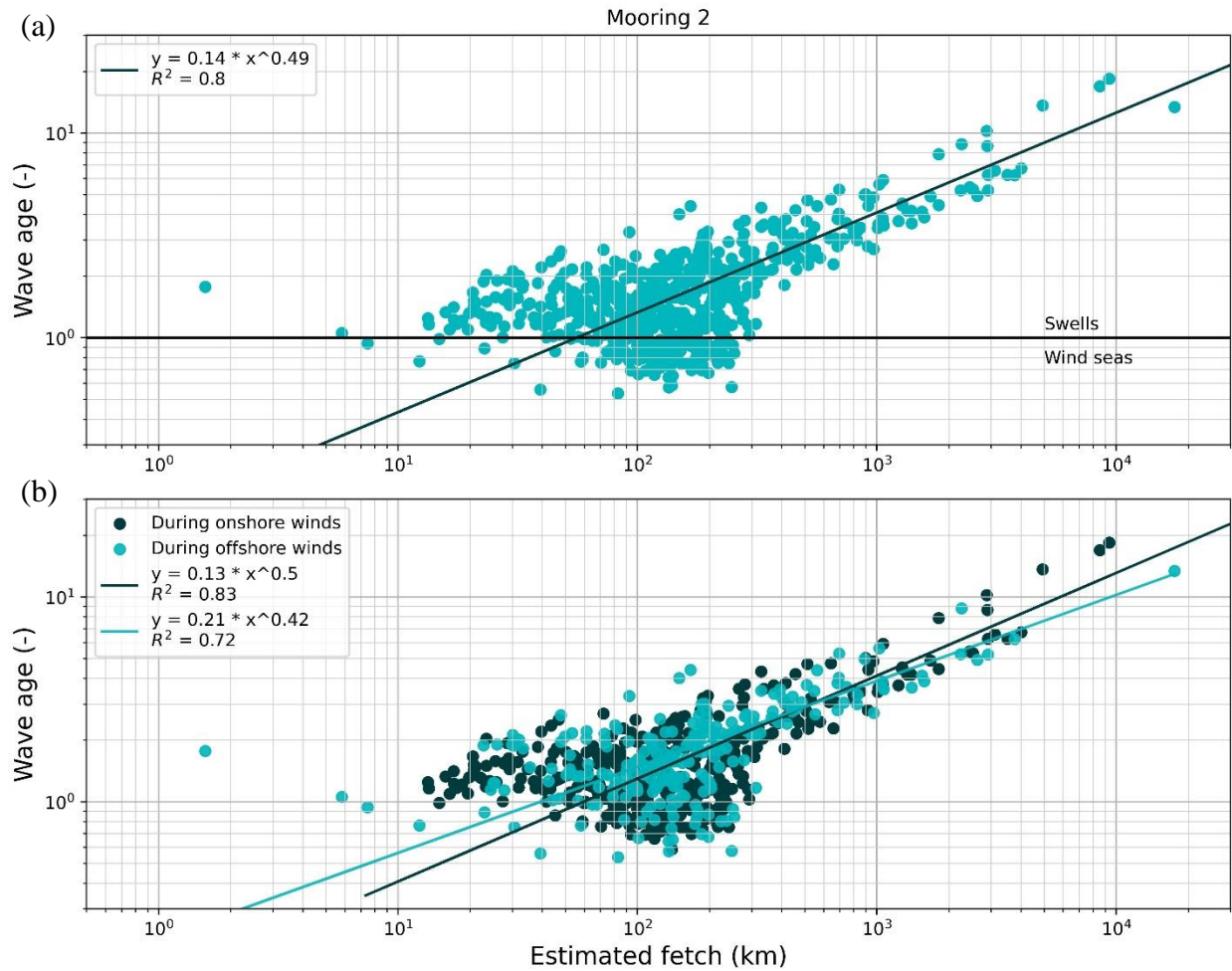


Figure 28. The wave age plotted with estimated fetch and fit with a power law relation for Mooring 2. (a) describes all of Mooring 2's data while (b) categorizes the data by wind direction and fits them separately. Onshore winds demonstrate the best power law fit with an  $R^2$  value of 0.83.

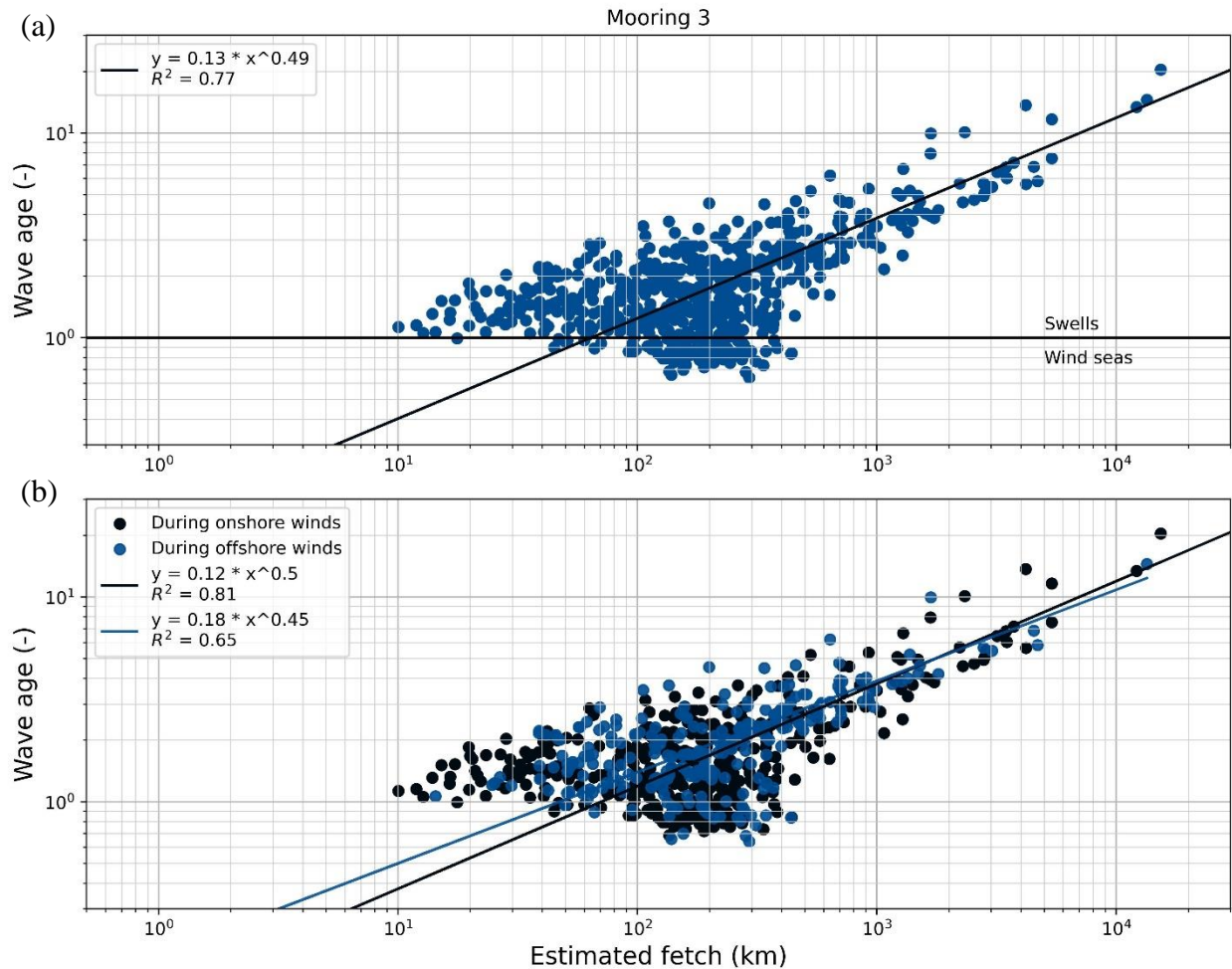


Figure 29. The wave age plotted with estimated fetch and fit with a power law relation for Mooring 3. (a) describes all of Mooring 3's data while (b) categorizes the data by wind direction and fits them separately. Onshore winds demonstrate the best power law fit with an  $R^2$  value of 0.81.

For all three moorings, onshore winds have the highest power law correlation with the highest  $R^2$  values (Table 2). This indicates that more developed waves correspond to greater fetch lengths, especially for onshore winds.

#### 4.3.2. Comparing locations

The trends described in the previous section apply to each mooring separately, but the relations between the moorings are also important. The spatial aspect is investigated by layering Figure 27a, Figure 28a, and Figure 29a in Figure 30. As the distance from shore increases from Mooring 1 to Mooring 3, the data shift towards longer fetches and higher wave ages.

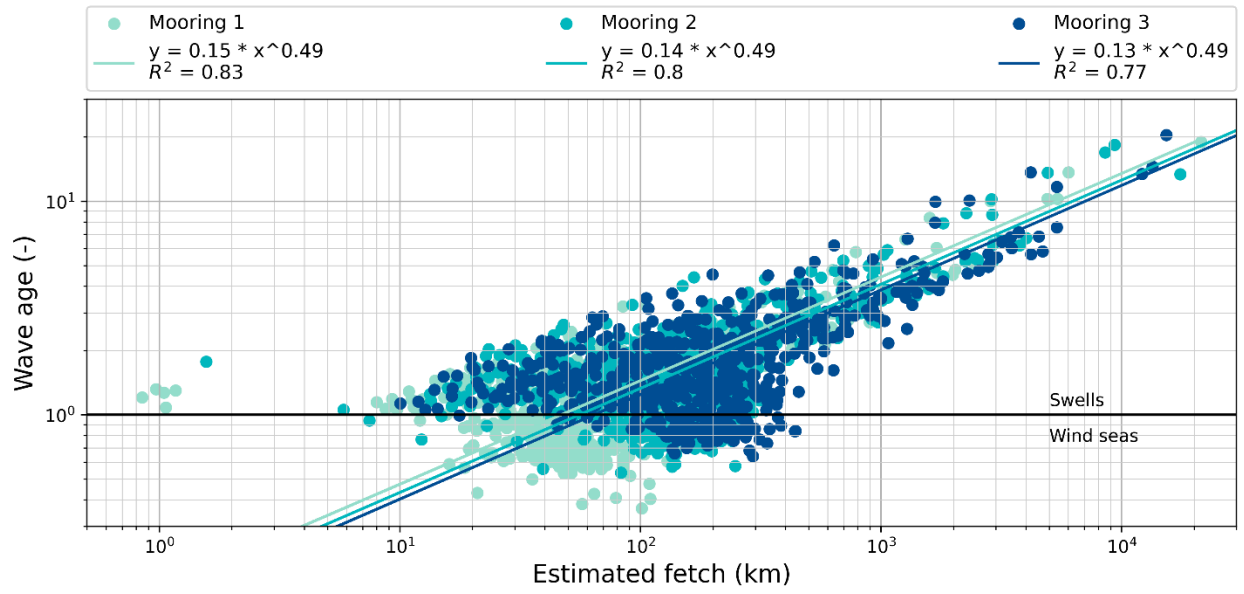


Figure 30. Results from all three moorings (Figure 27-29) using all data are layered to show how the bulk of the data shifts from Mooring 1 to Mooring 3. As distance from shore increases, the data shifts towards longer fetches and higher wave ages.

## 5. Conclusions and future work

This research investigates the development of waves in the coastal Arctic in three ways.

1. Study of waves directly limited by the mooring's distance from the coast show estimated fetches follow the expected increasing progression with offshore distance. The wave spectra of these instances exhibit more energy at higher frequencies and increasing peak energy with increasing distance from shore which are demonstrative of fetch-limited wave growth. This indicates fetch-limited wave growth between locations.
2. Comparisons of wave age and inferred fetch suggest the role of distance in development of waves. Power law fits of the wave age versus the fetch, indicate that for all three moorings more developed waves correspond to longer fetches, especially for onshore winds.
3. Across moorings, it is also observed that waves are more developed with further distances from shore.

In conclusion, the results indicate that fetch size limits wave growth, as theory suggests, and drives variability among coastal Arctic locations.

This research does not strive to solve climate change but adds to the cumulative understanding of air-sea-ice interactions in the Arctic. By corroborating expected relationships in fetch-limited wave growth, this research indicates that with increasing fetch lengths predicted by climate scientists, waves will evolve to be more developed at coastlines. This is especially relevant for onshore winds which correlate the best to the power law relation with estimated fetch and do not have physically limiting shores, like offshore winds.

### 5.1. Future work

This research works with new data collected as of September 2023, and thus there is still much that can be investigated with the dataset. This research provides preliminary analysis of the dataset and has the potential for a wide range of future directions. Avenues for future work include the incorporation of satellite products for ice. NASA Worldview satellite imagery provided the main source of ice observations in this analysis. However, cloud cover often obscured the image. In sea ice products visual imagery is often offset with radiometry data from microwave observations which provide coverage during cloudy and night-time conditions (*Arctic Sea Ice Measurements*, n.d.; *Near-Real-Time DMSP SSMIS Daily Polar Gridded Sea Ice Concentrations, Version 2*, 2020). Ice concentrations from higher-resolution products such as microwave or synthetic aperture radar (SAR) could be used to estimate fetches to quantitatively probe how sea ice limits fetches in the Arctic. A product with higher resolutions than ERA5 would be preferred to distinguish differences between moorings.

Another future avenue is the exploration of other atmospheric conditions during specific time periods, such as the increase in wave activity on Aug. 23<sup>rd</sup>, 2023, for a more refined interpretation of such events. Air temperature and surface pressure could be probed for relations

with the wave data, estimated fetches, and wave age. These atmospheric conditions can be signs of certain weather patterns which are most likely to drive events in the wave observations.

Future work could also compare past or future records of waves observed at this location to this analysis to determine if the results described here are generalizable or specific to 2023. Similarly, wave observations at other locations along the Alaska North Slope could be investigated to discern if the results described here are specific to this location or its geometry. This larger sample size would strengthen the significance of these results.

## 6. References

- Arctic Sea Ice Measurements*. (n.d.). National Centers for Environmental Information (NCEI). Retrieved April 24, 2024, from <https://www.ncei.noaa.gov/access/monitoring/dyk/arctic-ice>
- Brewster, K. (n.d.). *A Jukebox of Oral History—Northern Alaska Sea Ice Observations Through Time*. Retrieved December 11, 2023, from <https://www.arcus.org/witness-the-arctic/2015/2/article/23167>
- Colab.google*. (n.d.). Colab.Google. Retrieved April 22, 2024, from <http://0.0.0.0:8080/>
- Cooley, S. W., & Ryan, J. C. (2024). Community-scale changes to landfast ice along the coast of Alaska over 2000-2022. *Environmental Research Letters*. <https://doi.org/10.1088/1748-9326/ad1c7b>
- Cooper, V. T., Roach, L. A., Thomson, J., Brenner, S. D., Smith, M. M., Meylan, M. H., & Bitz, C. M. (2022). Wind waves in sea ice of the western Arctic and a global coupled wave-ice model. *Philosophical Transactions of the Royal Society A: Mathematical, Physical and Engineering Sciences*, 380(2235), 20210258. <https://doi.org/10.1098/rsta.2021.0258>
- Hersbach, H., Bell, B., Berrisford, P., Biavati, G., Horányi, A., Muñoz Sabater, J., Nicolas, J., Peubey, C., Radu, R., Rozum, I., Schepers, D., Simmons, A., Soci, C., Dee, D., & Thépaut, J.-N. (2023). *ERA5 hourly data on single levels from 1940 to present* [dataset]. Copernicus Climate Change Service (C3S) Climate Data Store (CDS). <https://doi.org/10.24381/cds.adbb2d47>
- Hošeková, L., Eidam, E., Panteleev, G., Rainville, L., Rogers, W. E., & Thomson, J. (2021). Landfast Ice and Coastal Wave Exposure in Northern Alaska. *Geophysical Research Letters*, 48(22). <https://doi.org/10.1029/2021GL095103>

Mahoney, A. R. (2018). Landfast Sea Ice in a Changing Arctic. *Arctic Report Card 2018*.  
[www.arctic.noaa.gov/Report-Card](http://www.arctic.noaa.gov/Report-Card)

Mahoney, A. R., Eicken, H., Gaylord, A. G., & Gens, R. (2014). Landfast sea ice extent in the Chukchi and Beaufort Seas: The annual cycle and decadal variability. *Cold Regions Science and Technology*, 103, 41–56. <https://doi.org/10.1016/j.coldregions.2014.03.003>

Meier, T. L. S., Grace Weikert, and Walt. (2023, September 25). *NASA Scientific Visualization Studio | Arctic Sea Ice Minimum 2023*. NASA Scientific Visualization Studio.  
<https://svs.gsfc.nasa.gov/5162/>

*NASA Worldview*. (2023). <https://worldview.earthdata.nasa.gov>

National Weather Service. (2018, December 13). *Product Descriptions*. National Oceanic and Atmospheric Administration; NOAA National Centers for Environmental Prediction.  
<https://polar.ncep.noaa.gov/waves/products.shtml?>

*Near-Real-Time DMSP SSMIS Daily Polar Gridded Sea Ice Concentrations, Version 2*. (2020, October 21). National Snow and Ice Data Center. <https://nsidc.org/data/nsidc-0081/versions/2>

*New to waves? Here's everything you need to know*. (n.d.). Nortek. Retrieved December 11, 2023, from <https://www.nortekgroup.com/knowledge-center/wiki/new-to-waves>

NOAA. (2023, January 20). *Why does the ocean have waves?* National Ocean Service Website.  
<https://oceanservice.noaa.gov/facts/wavesinocean.html>

NSIDC. (n.d.). *Science of Sea Ice*. National Snow and Ice Data Center. Retrieved January 11, 2024, from <https://nsidc.org/learn/parts-cryosphere/sea-ice/science-sea-ice>

- Ocean Physics at NASA - NASA Science*. (n.d.). Retrieved December 11, 2023, from <https://science.nasa.gov/earth-science/focus-areas/climate-variability-and-change/ocean-physics/>
- Open Lead | Project Jukebox*. (n.d.). Retrieved February 9, 2024, from <https://jukebox.uaf.edu/media-gallery/detail/2821/15224>
- Petrich, C., Eicken, H., Zhang, J., Krieger, J., Fukamachi, Y., & Ohshima, K. I. (2012). Coastal landfast sea ice decay and breakup in northern Alaska: Key processes and seasonal prediction. *Journal of Geophysical Research: Oceans*, 117(C2), n/a-n/a. <https://doi.org/10.1029/2011JC007339>
- Pizzo, N., Deike, L., & Ayet, A. (2021). How does the wind generate waves? *Physics Today*, 74(11), 38–43. <https://doi.org/10.1063/PT.3.4880>
- Raichlen, F. (2013). *Waves*. The MIT Press.
- R/V Tioga—Woods Hole Oceanographic Institution. (n.d.). <https://www.whoi.edu/>. Retrieved April 25, 2024, from <https://www.whoi.edu/what-we-do/explore/ships/ships-tioga/>
- Setchell, H. (2020, February 19). *ECMWF Reanalysis v5*. ECMWF. <https://www.ecmwf.int/en/forecasts/dataset/ecmwf-reanalysis-v5>
- Smith, M., & Thomson, J. (2016a). Scaling observations of surface waves in the Beaufort Sea. *Elementa: Science of the Anthropocene*, 4, 000097. <https://doi.org/10.12952/journal.elementa.000097>
- Smith, M., & Thomson, J. (2016b). Scaling observations of surface waves in the Beaufort Sea. *Elementa: Science of the Anthropocene*, 4, 000097. <https://doi.org/10.12952/journal.elementa.000097>

- Squire, V. A. (2007). Of ocean waves and sea-ice revisited. *Cold Regions Science and Technology*, 49(2), 110–133. <https://doi.org/10.1016/j.coldregions.2007.04.007>
- Squire, V. A. (2020). Ocean Wave Interactions with Sea Ice: A Reappraisal. *Annual Review of Fluid Mechanics*, 52(1), 37–60. <https://doi.org/10.1146/annurev-fluid-010719-060301>
- Squire, V. A., Dugan, J. P., Wadhams, P., Rottier, P. J., & Liu, A. K. (1995). Of Ocean Waves and Sea Ice. *Annual Review of Fluid Mechanics*, 27, 115–168.
- The Geophile Pages*. (n.d.). Retrieved December 12, 2023, from [https://geophile.net/Lessons/waves/waves\\_02.html](https://geophile.net/Lessons/waves/waves_02.html)
- Thomson, J., & Rogers, W. E. (2014). Swell and sea in the emerging Arctic Ocean. *Geophysical Research Letters*, 41(9), 3136–3140. <https://doi.org/10.1002/2014GL059983>
- Thomson, J., & Smith, M. (2024). *Moorings along the seafloor cable route extending offshore from Oliktok Point, Alaska, from April to September of 2023*. <https://doi.org/10.18739/A24J0B01J>
- US EPA, O. (2016, July 1). *Climate Change Indicators: Snow and Ice* [Reports and Assessments]. <https://www.epa.gov/climate-indicators/snow-ice>
- U.S. Navy Corps of Engineers. (2008). *Coastal Engineering Manual*. U.S. Navy Corps of Engineers.
- Webb, P. (2023). *Introduction to Oceanography*. Pressbooks. <https://rwu.pressbooks.pub/webboceanography/>
- Why Sea Ice Matters*. (n.d.). National Snow and Ice Data Center. Retrieved April 25, 2024, from <https://nsidc.org/learn/parts-cryosphere/sea-ice/why-sea-ice-matters>
- Young, I. R. (1999). Fetch and Duration Limited Growth. In *Elsevier Ocean Engineering Series* (Vol. 2, pp. 83–131). Elsevier. [https://doi.org/10.1016/S1571-9952\(99\)80007-5](https://doi.org/10.1016/S1571-9952(99)80007-5)